https://doi.org/10.5194/hess-2020-371
Preprint. Discussion started: 3 August 2020

Hydrology and Earth System Sciences
Discussions

On the value of high density rain gauge observations for small Alpine headwater catchment hydrology

Anthony Michelon[1], Lionel Benoit[1], Harsh Beria[1], Natalie Ceperley[1,2], Bettina Schaefli[1,2]

[1] Institute of Earth Surface Dynamics (IDYST), Faculty of Geosciences and Environment, University of Lausanne, Lausanne, 1015, Switzerland
[2] Now at: Institute of Geography (GIUB), Faculty of Science, University of Berne, Switzerland

Correspondence to: Anthony Michelon (anthony.michelon@unil.ch)

Abstract.

Spatial rainfall patterns exert a key control on the catchment scale hydrologic response. Despite recent advances in radar-based rainfall sensing, rainfall observation remains a challenge particularly in mountain environments. This paper analyzes the importance of high-density rainfall observations for a 13.4 km^2 catchment located in the Swiss Alps where rainfall events were monitored during 3 summer months using a network of 12 low-cost, drop-counting rain gauges. We developed a data-based analysis framework to assess the importance of high-density rainfall observations to help predict hydrologic processes. The framework involves the definition of spatial rainfall distribution metrics based on hydrological and geomorphological considerations, and the analysis of how these metrics explain the hydrologic response in terms of runoff coefficient and lag time. The gained insights are then used to investigate the optimal raingauge network density for predicting the hydrological metrics in the studied catchment. The analysis unravels that besides amount and intensity, the rainfall distance from the outlet along the stream network is a key spatial rainfall metric. This result calls for more detailed observations of stream network expansions, as well as the parameterization of along stream processes in rainfall-runoff models. In addition, despite the small spatial scale of this case study, the results show that an accurate representation of the rainfall field is of prime importance to capture the key characteristics of the hydrologic response in terms of generated runoff volumes and delay. In the present case, at least three rain gauges were required for proper runoff prediction.

1 Introduction

Rainfall is known to be highly variable in space even at small scales, in particular in mountain areas (Henn et al., 2018;Tetzlaff and Uhlenbrook, 2005). Despite recent progress in the observation of spatial rainfall with the help of radar (Berne and Krajewski, 2013;Germann et al., 2006;Germann et al., 2015), it remains crucially difficult to observe and spatially interpolate (Foehn et al., 2018a;Sideris et al., 2014).

Understanding the interrelation between spatial rainfall patterns and the hydrologic response has been of concern for many decades, ranging from a theoretical viewpoint (Shah et al., 1996;Singh, 1997;Woods and Sivapalan, 1999), to a rainfall-runoff model perspective (Obled et al., 1994;Nikolopoulos et al., 2011), and extending to a hydrological process understanding

https://doi.org/10.5194/hess-2020-371
Preprint. Discussion started: 3 August 2020


Hydrology and Earth System Sciences
Discussions

perspective (Guastini et al., 2019;Zillgens et al., 2007). Even earlier work in this field focused on the model-based investigation of optimal rain gauge density for reliable areal rainfall estimation (Bras and Rodriguez-Iturbe, 1976a) and runoff prediction (Bras and Rodriguez-Iturbe, 1976b;Tarboton et al., 1987). Chacon-Hurtado (2017) provides a recent review on rain gauge network optimisation.

A wide range of methods has been proposed to analyze the hydrologic response as a function of spatial rainfall patterns. We can broadly distinguish between empirical methods that identify systematic response patterns by scrutinizing individual observed events (Blume et al., 2007) and model-based methods that try to identify systematic or theoretical relationships between rainfall and the hydrologic response. In this latter category, we first of all find stochastic methods that describe the stochastic aspects of the hydrologic response as a function of the rainfall field properties. These approaches range from simplified stochastic models (Tarboton et al., 1987) to full space-time representations of rainfall forcing and streamflow generation (Mei et al., 2014;Pechlivanidis et al., 2017;Viglione et al., 2010;Woods and Sivapalan, 1999;Zoccatelli et al., 2015). These stochastic tools are developed to understand the relative importance of the two key components of the hydrologic response, i) the runoff generation processes at the hillslope scale and ii) the routing mechanisms in the channel network. Such an assessment of the relative role of unchanneled-state and channeled-state processes (Rinaldo et al., 1991;Rinaldo et al., 2006a) gives key insights into the relative role of runoff generation processes and the geomorphology of a catchment. This can also be achieved with virtual modelling experiments with hydrological models that explicitly account for geomorphological dispersion along the channel network. An example is the work of Nicótina et al. (2008) who assessed the importance of well representing spatial rainfall variability for medium size catchments (a few hundreds to thousands km^2) where saturation-excess overland flow dominates (rather than Hortonian flow). They conclude that for rainfall events with a spatial correlation length larger than the hillslope size, an exact representation of the spatial rainfall variability is not required to well represent the hydrologic response - provided that the mean areal rainfall is preserved at each time step. They explain this result by the fact that if the total catchment-scale residence time is controlled by the travel time within the hillslopes, large enough rainfall events sample all possible residence times, independent of the actual spatial rainfall configuration. Their findings were subsequently confirmed by the work of Volpi et al., (2012) amongst others, where a simplified modelling approach based on a geomorphological unit hydrograph was used. While the conclusions were similar, this study also added that spatial variability does not matter "when the integral scale of the excess-rainfall field is much smaller or much larger than the basin drainage area".

Similar results were obtained in studies that assess the impact of undersampling or of coarse graining an observed rainfall field on the performance of streamflow simulations obtained with more or less complex process-based hydrologic models (Bardossy and Das, 2008;Moulin et al., 2009;Lobligeois et al., 2014;Shah et al., 1996;St-Hilaire et al., 2003;Stisen and Sandholt, 2010;Xu et al., 2013). A key result of these model-based studies is that the hydrologic response depends more on the accurate estimate of the mean areal rainfall than on the actual exact form of the rainfall field, (Obled et al., 1994). However, such model-based studies face the challenge that conceptual hydrological models require recalibration when used with different input fields,

https://doi.org/10.5194/hess-2020-371
Preprint. Discussion started: 3 August 2020


Hydrology and Earth System Sciences
Discussions

which makes disentangling effects from rainfall versus parameters a cumbersome exercise (Bardossy and Das, 2008;Bell and Moore, 2000;Stisen and Sandholt, 2010).

The above hypothesis that the area-average rainfall might play a more important role for the streamflow response than the actual spatial rainfall pattern remains to be tested in the field. In this paper, we propose a data-based analysis of the importance of rain gauge density for the event-specific hydrologic response (Ross et al., 2019) of a small, high elevation Alpine headwater catchment (13.4 km^2) where the hydrologic processes have been intensely monitored since 2015. Such a small catchment has potential to shed new light on the assumption that for catchments smaller than a few tens of km^2, a single rain gauge is sufficient for reliable runoff prediction.

To assess the number of point observations required to properly capture the hydrologic response of our target catchment, we set up a dense rain gauge network made of commercially available and low cost devices, which increases the interest of this case study for future hydrologic studies in similar settings. These high density rain gauge observations (approximately one rain gauge per km^2) are then used to answer two key questions:

i. Which spatial characteristics of the rainfall field explain the timing and the amplitude of the hydrologic response?
ii. What is the required spatial design of the rain gauge network to capture these characteristics?

To answer these questions, we developed a methodological framework to analyze the rainfall events, the hydrological response, and ultimately the optimal rain gauge density. This framework can be summarized as follows: i) define appropriate metrics to describe the rainfall fields and the hydrological response, ii) understand the relationships between these metrics through correlation analysis, iii) identify the main drivers (i.e. the corresponding metrics) through regression analysis, and finally iv) use the gained insights to optimize the rain gauge network based on selected metrics.

The remainder of the paper is structured as follows. First, Section 2 describes the target area of the study, namely the Vallon de Nant catchment located in the Western Swiss Alps. Next, Section 3 presents the observational methods and the analysis framework. The results are presented in Section 4 and discussed in Section 5, with a focus on the impact of rainfall heterogeneity on the streamflow response. Section 6 summarizes the main conclusions.

2 Study area

The area of interest is the Vallon de Nant, a 13.4 km^2 catchment located in the Western Swiss Alps (Figure 1). The elevation ranges from 1,200 m asl. at the outlet of the Avançon de Nant river (Figure 2) to 3,051 m asl. (Grand Muveran), and has an average elevation of 1,975 m asl. The catchment benefits from a protected status (Natural Reserve of the Muveran) since 1969 and is of national importance for Switzerland in terms of biodiversity (Cherix and Vittoz, 2009). The Vallon de Nant has been intensively studied over the recent years, in disciplines ranging from hydrogeology (Thornton et al., 2018), to pedology (Lane et al., 2016;Rowley et al., 2018), to biogeochemical cycling (Grand et al., 2016), and to stream ecology (Horgby et al., 2019).

The Vallon de Nant belongs to the reverse side of the Morcles nappe, a structural geological unit that determines the catchment's shape. The old Cretaceous and Tertiary layers are recognizable as a succession of thick, blocky lithologies

https://doi.org/10.5194/hess-2020-371
Preprint. Discussion started: 3 August 2020


Hydrology and Earth System Sciences
Discussions

overlooking and surrounding the valley. They lie on a substratum of flysch, i.e. softer rocks (schistose marls and sandstone benches), which explains the deepening and widening of the valley at its southern part (Badoux, 1991).

Figure 3 summarizes the dominant hydrological units of the Vallon de Nant. The western side is mainly characterized by grassy slopes, with deep soils and a relatively high water storage capacity as revealed by gauging along the stream during the late summer and autumn yearly streamflow recession period (Horgby, 2019). The northern part of these western slopes shows a less dense drainage network than the rest of the catchment (Figure 1), explained by steeper slopes, a large hydraulic conductivity or locally deeper soils.

The eastern side of the catchment is characterized by steep and rocky slopes that react quickly to rain events due to shallow soils that drain quickly. At the foot of the rock walls, large alluvial cones and screes extend down to the river. The bottom of the valley is mainly composed of fine alluvial deposits with a large water storage capacity. In the southern part of the valley, the Glacier des Martinets (area less than 1 km^2) is now confined to a small area shaded by the Dents de Morcles. The water flow paths of rainfall inputs over this southern (and higher elevation) part of the catchment, composed of moraines and permafrost, remain unclear and have not been investigated so far.

The Avançon de Nant river shows a typical snow dominated streamflow regime marked by a high flow period during spring and early summer when the snowpack accumulated during the winter melts (Supplementary Material Figure S1). The river length within the study area reaches 6 km in early summer, while during autumn and winter low flow, the river may start to flow as low as 1480 m asl. (close to the gauge No. 5 on the Figure 1), reducing the instream flow distance to the outlet to 2.95 km. The actual extent of the stream network is based on observations during dry and wet periods during Summer 2017 and its exact path was calculated using the Swiss digital elevation model at a resolution of 2 m (swissALTI3D, 2012).

The streamflow at the outlet is monitored via river height measurements using a sonar above the middle point of a trapezoidal shaped weir (Figure 2). It averages water height every 1 minute continuously since September 2015. The height is then converted into streamflow using a rating curve (Supplementary material Figure S3) based on 55 salt streamflow measurements (Ceperley et al., 2018). We fit a power-relationship using the nonlinear least squares fitting algorithm of MatLab's "fit" function with the trust region algorithm and least absolute residual method to obtain a 95% confidence interval. The annual average streamflow in 2018 is between 0.60 and 0.72 $m^3.s^{-1}$ (between 3.89 and 4.61 $mm.day^{-1}$); average annual water temperature is 5.0°C, ranging from a frozen river during some days in winter to an average temperature of 8.5°C during summer (from July 1st to August 31st, 2017). The maximum streamflow measured at the gauging station was between 10.4 and 12.4 $m^3.s^{-1}$ (between 67.2 and 80.0 $mm.day^{-1}$) during an intense rainfall event (August 6th, 2018).

Meteorological variables are monitored at three locations (Michelon et al., 2017) along a north/south transect (at 1253 m asl., 1530 m asl. and 2136 m asl.) since September 2016. The average air temperature at mean elevation estimated from these stations equals 3.1 °C in 2017.

We do not use any further data from the Swiss meteorological network since there are no ground measurement stations nearby, and the Vallon de Nant catchment is largely in the shadow of the Swiss weather radar network (Foehn et al., 2018b), which might see here at best rainfalls above 2800 m asl. (Marco Gabella personal communication, February 27th 2019).

https://doi.org/10.5194/hess-2020-371
Preprint. Discussion started: 3 August 2020


Hydrology and Earth System Sciences
Discussions

3 Instruments and methods

3.1 Instruments

A network of 12 Pluvimate drop-counting rain gauges (www.driptych.com) was distributed across the Vallon de Nant catchment from July 1st to September 23rd 2018 to monitor rainfall (Figure 1). A similar deployment during the cold season would not be possible due to snowfall at all elevations throughout the winter. The sites were selected to represent the distribution of slope orientations and elevation, but also to meet constraints of accessibility and disturbance risk (livestock, hikers). The distance between measurement locations within the network ranges from 350 m to 1,550 m (630 m on average), and the greatest distance from any point in the basin to a rain gauge is 1,670 m.

The gauges are low-cost (around 600 USD each), consisting of a tube (11 cm of diameter, 40 cm of length) mounted to an aluminum funnel (Figure 4). The collected rainwater is concentrated to a nozzle that creates a drop of water of calibrated size (0.125 mL), which then falls on the impact-sensitive surface of the sensor, 30 cm below. The datalogger counts and records the number of drops over a time set up to 2 minutes. In the field, the devices are set up vertically, attached to a wooden stick. The funnel aperture is between 0.8 and 1.2 m above the ground.

The Pluvimates were set-up to count drops over an interval of 2 minutes, with an accuracy of 0.3 mm/h. Benoit et al. (2018a) experimentally evaluated the device uncertainty to 5 % for rainfall intensities under 20 mm/h. Given that some of the rainfall intensities measured in the present study exceed this value (intensities up to 140 mm/h were recorded), we extended the calibration to intensities up to 150 mm/h, and few saturation effects were noticed (Appendix A).

To prevent clogging, steel sponges were disposed in the funnel of each Pluvimate. This appeared to have caused i) a dampening effect on low rainfall intensities as it delayed slightly the beginning of events (lower than 1 mm/h) and ii) created drops remaining after the end of an event. The data are not corrected for these effects.

Some additional artefacts were recorded, probably generated by strong winds creating resonance. These periods have been manually removed from the data.

3.2 Rainfall events

3.2.1 Event identification

Before further analysis, the rainfall amounts measured by each station were interpolated to a 10 by 10 m grid at a 2 min time step using a high-resolution stochastic interpolation procedure developed by Benoit et al. (2018). In a nutshell, it aims at generating an ensemble of stochastic space-time rain fields constrained by the actual observations at raingauge locations (over 20 realizations), and to use this ensemble to interpolate sparse rain observations.

Using the interpolated rainfall fields, rainfall events were identified as rainy periods separated by at least 90 minutes without rain. This inter-event duration was selected based on the observed delay between rainfall onset and streamflow response for the large event recorded on August 23rd (detailed in the part 2 of supplementary material); the streamflow reaction to the first half-hour of this rainfall event was caused only by rainfall in the southern half of the catchment (stations 8 to 12). Ninety

https://doi.org/10.5194/hess-2020-371
Preprint. Discussion started: 3 August 2020


Hydrology and Earth System Sciences
Discussions

minutes was therefore selected to maximize the chances of observing a distinct streamflow reaction for two distinct consecutive events. In addition, events with a total amount of rainfall under 1 mm are overlooked in the following.

3.2.2 Spatial rainfall pattern metrics

To investigate the relationship between dominant spatial rainfall patterns and streamflow response, the catchment is split into two parts of equal area by a west-east line (Figure 1), delimiting an area close to the outlet in the northern part, and an area farther away in the southern part. The interpolated amounts of rainfall received by the southern and northern parts of the catchment, P_{NORTH} and P_{SOUTH}, are compared and normalized by the total amount of rainfall to create an index of spatial rainfall asymmetry I_{ASYM}:

$$I_{ASYM} = \frac{P_{SOUTH} - P_{NORTH}}{(P_{SOUTH} + P_{NORTH})}, \quad (1)$$

If rainfall is equally distributed between the northern and the southern parts, then $I_{\mathrm{ASYM}} = 0$. The extreme values -1 and 1 express rainfall concentration exclusively in the northern or the southern part of the catchment, respectively. We consider a rainfall event as asymmetric when at least 2 times more rain is precipitated over one part of the catchment than over the other, i.e. when I_{ASYM} is below -0.33 or above +0.33.

To further analyze the relationships between the spatial distribution of rainfall and the streamflow response, we characterize the geomorphological distance of incoming rainfall from the outlet, assuming that this distance should reflect to some degree the timing and the shape of the streamflow reaction of the catchment: following the terminology of Rinaldo et al. (2006b), transport at the basin scale can be analyzed in terms of travel in the unchannelled state (i.e. in the hillslopes) and travel in the channelled state (i.e. in the stream network).

Accordingly, we estimate for each rainfall event the weighted average unchannelled distance to the stream network as:

$$D_{HILLS} = \frac{1}{t}\sum_t \frac{\sum_i \sum_j P(i,j,t) d_{HILLS}(i,j)}{\sum_i \sum_j P(i,j,t)}, \quad (2)$$

where t is the time step, i and j are the coordinates of rainfall location within the grid, and $d_{HILLS}(i,j)$ is the distance of this grid cell to the nearest stream network grid cell (following the line of steepest descent in the 2 x 2 m DEM (swissALTI3D, 2012)).

Similarly, we compute the weighted average channelled distance between a point of introduction into the stream network and the outlet as:

$$D_{STREAM} = \frac{1}{t}\sum_t \frac{\sum_i \sum_j P(i,j,t) d_{STREAM}(i,j)}{\sum_i \sum_j P(i,j,t)}, \quad (3)$$

where $d_{STREAM}(i,j)$ is the distance along the stream network from the point of introduction to the outlet. For each cell of the stream network, this distance is calculated once based on the 2 x 2 m DEM.

The D_{HILLS} metric gives an estimate of the average distance that incoming rainfall has to travel on the hillslopes before reaching the stream network, and D_{STREAM} the average distance for the water particle entering the stream network to reach the outlet.

https://doi.org/10.5194/hess-2020-371
Preprint. Discussion started: 3 August 2020


Hydrology and Earth System Sciences
Discussions

In addition to the above two metrics related to the theory of geomorphological dispersion (Rinaldo et al., 2006b), we use the height above the nearest drainage (HAND) terrain metric (Renno et al., 2008;Gharari et al., 2011;Nobre et al., 2011) to account for the topography. Based on the 2 x 2 m DEM, the normalized terrain heights d_{HAND} are calculated by comparing the elevation of each grid cell to the elevation of the nearest stream network cell in which the water is routed. The average HAND value for a rainfall event is given by:

$$D_{HAND} = \frac{1}{t}\sum_t \frac{\sum_i \sum_j P(i,j,t) d_{HAND}(i,j)}{\sum_i \sum_j P(i,j,t)}. \quad (4)$$

Since the extent of the stream network is dynamic, its minimal and maximal extent (Figure 1) are determined manually by identifying the uppermost points of the catchment where streamflow has been observed in the field during summer baseflow (minimum extent) and during high flow (maximum extent). The 3 distance metrics are computed with respect to both network extents; the network extent to be used per rainfall event is then determined during the rainfall-streamflow response analysis (Section 3.5).

3.3 Streamflow response

3.3.1 Event identification

The beginning and the end of each streamflow event are identified manually using a data visualization tool (developed in Mathworks MatLab 2017a, see Figure 5 and Figure 6). This choice of a visual expertise was made based on the observation that automatic identification of streamflow events would require almost a case-by-case filtering and parametrization, and thus would not be generalizable. This is partly related to a potentially high signal-to-noise ratio for river stage recordings during sediment transport events, a phenomenon potentially very important after a strong streamflow variation. The result of this visual identification for each streamflow event is displayed in the part 2 of Supplementary Material.

The beginning and the end of the streamflow response determine the initial and final baseflow, respectively; the streamflow volume above the line connecting these two points is considered here as fast runoff. It is noteworthy that we do not use peak streamflow to characterize streamflow events, for two reasons: i) given the small size of the catchment and the complex temporal distribution of rain intensities, the streamflow response has rarely a single, well identifiable peak; ii) peak streamflow identification is further complicated by the noise in the stage recordings.

3.3.2 Streamflow metrics

To characterize the hydrologic response in terms of streamflow volume and timing, we use the runoff coefficient and the lag time, the two key characteristics of streamflow reaction. The runoff coefficient (RC) is obtained by dividing the fast runoff by the total rainfall for the given event. A metric for the elapsed time between the rainfall event and the streamflow reaction is obtained as the lag between the moment when one third of the rainfall event has fallen and when one third of the corresponding streamflow volume has passed the gauge and is called $\Delta_{\mathrm{P/Q}}$. Given the visual assessment of the start of the streamflow event,

https://doi.org/10.5194/hess-2020-371
Preprint. Discussion started: 3 August 2020


Hydrology and Earth System Sciences
Discussions

this measure is deemed more robust than the elapsed time between the start of the event, and is indicative for the time when a significant part of the streamflow volume has reached the outlet.

3.4 Rainfall-streamflow response characterization

We analyze the relationships between the spatial distribution of rainfall and the hydrological response based on a correlation analysis of the above metrics, followed by a regression analysis to identify the key variables that explain the runoff coefficient and streamflow lag time. This analysis requires a measure for initial catchment wetness conditions, which are known to be the major variable explaining the dynamics of the hydrological response to different rainfall events (Penna et al., 2011;Rodriguez-Blanco et al., 2012), in particular through the creation of runoff thresholds (Zehe et al., 2005;Tromp-van Meerveld and McDonnell, 2006). Many studies use the baseflow before the start of a streamflow event as an indicator for the antecedent moisture state of the catchment. For snow-influenced catchments with a highly seasonal streamflow regime, this indicator might not reflect the actual saturation conditions. Hence, we rather quantify initial wetness conditions in terms of antecedent rainfall, i.e. using the cumulative rainfall (in mm) that occurred during a period from 1 to 5 days before an given rainfall event. All used metrics are summarized in Table 1.

We use a pure quadratic regression to investigate which rainfall pattern characteristics and initial wetness conditions are the best predictors of the runoff coefficient and the lag time. Pure quadratic regression (i.e. without multiplication of explanatory variables) is chosen because the small number of observed streamflow events prevents using more complex models. Model selection is performed using the Akaike Information Criterion (AIC)(Akaike, 1974), noted here as I_{AIC}:

$$I_{AIC} = n \ln\left(\frac{S_{RSS}}{n}\right) + 2k + C \,, \quad (5)$$

where n is the number of events, k the number of coefficients, S_{RSS} the residual sum of squares and C a constant that can be ignored when comparing different models based on the same data set. As we manage small sample sizes (Burnham et al., 2011), we compute and use a corrected version of the AIC (AICc, noted here I_{AICc}):

$$I_{AICc} = I_{AIC} + \frac{2k(k+1)}{n-k-1} \quad (6)$$

For both AIC and AICc, the best model is the one having the lowest score.

3.5 Measurement network configuration analysis

Assuming that the actual rainfall measurement network is sufficient to capture the full spatial distribution of rainfall in the studied catchment, we assess the ability of partial networks to reproduce the identified best explanatory variables. The aim is twofold: i) identifying the best configuration for a future permanent observation network and ii) evaluate the added value of additional rain gauges in a partial network with respect to the identified key metrics (Section 4.4 and 5.2).

The quality of a partial network configuration is evaluated comparing the value (e.g. total rainfall) by event obtained with the partial network to the reference value obtained with the full network setup. We evaluate all the possible combinations of partial

https://doi.org/10.5194/hess-2020-371
Preprint. Discussion started: 3 August 2020


Hydrology and Earth System Sciences
Discussions

networks composed of less than 12 stations, i.e. 4094 possibilities. Each configuration is evaluated based on the root mean square error (RMSE):

$$\text{RSME} := \sqrt{\sum_{\forall t} \frac{\left(X_k(t) - X_{ref}(t)\right)^2}{N}}, \quad (7)$$

where X_k is the selected rainfall metric (e.g. rainfall amount) at time step t corresponding to the k-th network configuration, X_{ref} the respective value obtained reference network set-up, and N the number of time steps. The rainfall amounts measured by each station were interpolated to a 10 by 10 m grid at a 2 min time step using the Thiessen polygons method. The interpolation method developed by Benoit et al. (see section 3.2) cannot be used in this context because i) it requires at least 5 measuring points to perform adequately and ii) the computation time would be excessive to explore the 4094 combinations of stations for each event.

The best network for each number of stations is the one with the lowest RMSE. A sensitivity analysis is completed by removing from 1 to 3 rainfall events to the 23 events dataset, yielding 2047 datasets evaluated for each partial network configuration. The most frequent network configuration validates the robustness of the result.

4 Results

4.1 Rainfall events

4.1.1 Amounts and asymmetry

The available 3-month measurements window between July 1st and September 23th 2018 captured 48 rain events (detailed in the part 2 of the Supplementary Material) for a total rainfall amount of 317.8 mm. The areal rainfall amount per event ranges from 1 mm to 43.5 mm, and event duration ranges from 32 minutes to 10.5 hours. Despite the sequential deployment of the 12 rain gauges and other technical issues (see section 3.1), the rainfall events were all measured by at least 7 stations; 36 out of 48 events were recorded by at least 10 stations and 23 events were recorded by 12 stations. Details for all recorded rainfall events and the corresponding streamflow are shown in summary plots, as illustrated in Figure 5 and Figure 6 (all events are presented in the Supplementary Material). Most events show a relatively homogeneous spatial distribution of rainfall events (see an example in Figure 6), with only few events showing a strong asymmetry (Figure 7): the correlation between P_{NORTH} and P_{SOUTH} equals 0.91, with an average I_{ASYM} of -0.01. Interestingly, strong spatial asymmetry mainly affects events with low rainfall amounts, with 7 out of 8 asymmetric events (when $|I_{ASYM}| > 0.33$) receiving below 5 mm (Figure 7). For the events that actually triggered a streamflow reaction, the correlation between P_{NORTH} and P_{SOUTH} is thus significantly lower (r=0.69, Table 3).

One strongly asymmetric and high intensity event occurred on July 24th at 6:32 PM (Figure 5). The rainfall map shows a heterogeneous distribution of rainfall, centered close to the outlet in the northern part of the catchment, over 6 out of the 12 stations. One of the rain gauges recorded up to 35.3 mm of rainfall, whereas 1.8 km upstream, half of the stations (on the southern and western parts of the catchment) did not record any rainfall. The interpolated amount of rainfall over the basin

https://doi.org/10.5194/hess-2020-371
Preprint. Discussion started: 3 August 2020


Hydrology and Earth System Sciences
Discussions

was 8.0 ± 1.3 mm, and a fast runoff volume between 28.3 and 32.5 mm was measured, resulting in a runoff coefficient between 3.0 and 4.8 that remains difficult to explain. One possible explanation is that important rainfall amounts fell on the north-eastern part of the catchment, over steep slopes that are difficult to access and were therefore not gauged. This event and its streamflow reaction are excluded from further analysis (see also Section 4.2).

4.1.2 Stream network distance metrics

For the 48 recorded rainfall events, all distance metrics show a significantly different distribution of the distances with respect to the wet network than with respect to the dry network; we can reject the hypothesis that the distributions have the same median value with a Wilcoxon rank sum test at level 0.05 (see distributions in Figures S4 and S5). The three distance metrics show a strong correlation between the wet and dry network state (from 0.94 for D_{HAND} to 1.00 for D_{STREAM}, Figure 8). The correlation between the distance metrics for the wet state range from 0.70 (D_{HILLS}- D_{STREAM}) to 0.95 (D_{HILLS} - D_{HAND}) and for the dry state from 0.75 (D_{STREAM} - D_{HAND}) to 0.95 (D_{HILLS} - D_{HAND}). For the events with streamflow reaction, these correlations are slightly lower (Table 3), but with a clear correlation between D_{HILLS} and D_{HAND} for the wet and dry state; accordingly, we do not further use the D_{HAND} metric in this analysis. None of the distance metrics shows a strong correlation (>0.6) with the rainfall spatial distribution metrics, i.e. P_{SOUTH}, P_{NORTH} or I_{ASYM}. They also do not show any correlation higher than 0.6 with the hydrologic response metrics (Table 3). This confirms our hypothesis that the network state needs to be included in a dynamic way (see Section 4.2.3).

4.2 Hydrologic response

4.2.1 Observed streamflow events

For 6 of the 48 rainfall events (13 days in total), the water stage sensor was disturbed by the proximity of a rock (see picture of the Figure S2 in the part 1 of the Supplementary Material), resulting in missing streamflow data. For the remaining 42 rainfall events, a streamflow response was observed for 15 of them (Table 2).

The fast streamflow volume during these events, $Q_{FAST,}$ shows a strong correlation with total rainfall and with P_{SOUTH} (Figure 9a); however, the event on 24 July with only 8.0 mm of rain and 30.4 mm of fast streamflow falls far away from this relationship, which further motivated the exclusion of this event from the analysis.

The 14 remaining events are distributed over the entire observation period, covering a wide range of streamflow conditions, which is reflected in the initial streamflow before each event, ranging from 7.9 mm in early July to 2.6 mm by mid-September (Table 2), with an almost linear decrease between the dates (correlation between initial streamflow and day of the year of -0.90, see also Figure S3 in the Supplementary Material S1).

The correlation of this initial flow before events with Q_{FAST} or with the runoff coefficient RC is extremely low (correlation of -0.02 and -0.05). The highest correlation between RC and antecedent precipitation occurs for a time span of 3 days preceding the streamflow event (0.67); this metric, called $W_{3\ days}$, is thus retained as a proxy for antecedent moisture for further analysis.

https://doi.org/10.5194/hess-2020-371
Preprint. Discussion started: 3 August 2020


Hydrology and Earth System Sciences
Discussions

The role of initial wetness conditions can also be discussed more qualitatively by comparing a pair of rainfall events with very similar spatial patterns and amounts (Figure 6). For the first event (24 August), the measured rainfall ranges from 6.2 mm to 11.8 mm, corresponding to 8.5 mm of rainfall over the catchment in 2 h 38 min. For the second event (29 August), the rainfall ranged between 5.4 mm and 11.4 mm, corresponding to 8.4 mm over the catchment during 1 h 14 min. Despite the similar total amount of rainfall and event duration (during the first event 76 % of the total rain happened for a duration similar to the second event), the first event shows a fast runoff volume of 7.4 mm, whereas for the second event the streamflow response is almost invisible. This difference can be explained by the initial wetness conditions, with 29.5 mm of rainfall during the 3 days preceding the first event, compared to 12.4 mm for the second event.

4.2.2 Streamflow generation processes, RC and lag

The strong correlation between rainfall amounts and Q_{FAST} (0.77, Table 3) suggests that streamflow reactions are triggered by saturation-excess, rather than by infiltration capacity-excess. This is confirmed by i) the absence of correlation between maximum rainfall intensity over 10 minutes and the RC (Table 3), ii) the strong correlation between rainfall duration and Q_{FAST} (0.73) and iii) by the clear threshold effect for the generation of streamflow as a function of total event rainfall (Figure 9); a streamflow reaction only occurs for total rainfall higher than 5 mm.

This threshold effect supports the formulation of the lag time (after the time when one third of the event volume has occurred) since a lag time between the starts of the events would here be misleading. Accordingly, the streamflow events show a relatively strong correlation (0.71) between the RC and the lag $\Delta_{P/Q}$: to reach a higher RC, we need a higher level of saturation, which results in a longer lag before a significant amount of streamflow reaches the outlet.

However, there is also a non-negligible negative correlation between $\Delta_{P/Q}$ and the maximum rainfall intensity over 10 minutes, especially with $P_{max\ NORTH}$ (r=-0.71, Table 3). This probably reflects the fact that in the northern part of the catchment, there is a lack of soil storage capacity due to the large rock walls on the right stream side, which is not compensated by the available soil storage on the left stream side, with ensuing Hortonian (infiltration-excess) streamflow generation processes becoming more dominant than in the southern part of the catchment. This significant difference in streamflow generation processes is also visible in the drainage density, which is much higher on the right stream side in the northern part (Figure 1).

4.2.3 Dynamic stream network state

Given the absence of correlation between the rainfall distance metrics and the hydrologic response, we attribute the network state to each streamflow event as a function of the antecedent wetness $W_{3\ days}$, as a measure for the stream network expansion. Setting a $W_{3\ days}$ threshold to 20 mm to discriminate between the dry and the wet state yields correlations between D_{HILLS} – composite and RC of -0.70, between D_{HILLS}-composite and $\Delta_{P/Q}$ of -0.66 (Table 4). D_{STREAM} –composite shows correlations of 0.53 and 0.60 with the RC and $\Delta_{P/Q}$ in this case, and we retain both composite distances for further analysis. A sensitivity test showed that setting a $W_{3\ days}$ threshold of between 12 mm and 20 mm to discriminate between the dry and the wet state yields very similar results, and we retain a threshold of 20 mm for W_{3days} to compose the combined network state. It should however

https://doi.org/10.5194/hess-2020-371
Preprint. Discussion started: 3 August 2020


Hydrology and Earth System Sciences
Discussions

be kept in mind that this composite distance metrics represent simply a heuristic solution to overcome the absence of detailed stream network state observations before each event. The resulting composite distance metrics do not show correlations >0.6 with the other rainfall metrics; accordingly, all rainfall metrics are retained for further analysis in addition to the composite distance metrics.

4.3 Identification of dominant hydrologic rivers via regression analysis

The above correlation analysis results in a range of potential explanatory variables for RC and $\Delta_{P/Q}$ referring to the rainfall amounts, intensity and asymmetry, the composite rainfall distance metrics and initial wetness conditions ($W_{3\ days}$). However, according to the correlation analysis, we retain the rainfall intensities as explanatory variables only for $\Delta_{P/Q.}$ The tested models are summarized in Table 5 for RC and in Table 6 for $\Delta_{P/Q}$. The analysis is based on 14 events (after removing the 24 July event).

In terms of AICc, the best ranked model for RC is a single predictor model using $D_{STREAMS}$ (composite) as explanatory variable, which yields better results than using antecedent moisture $W_{3\ days}$ as a single predictor; it should be kept in mind here that the composite distance metrics also embed information on antecedent moisture conditions (since $W_{3\ days}$ decides on the moisture state). However, the coefficient of determination (R^2) becomes considerably higher (0.75) using P_{ALL} and D_{STREAM} (composite) as explanatory variables. Slightly less good results are obtained with D_{HILLS} (composite) as a single predictor or in combination with P_{SOUTH}. The fact that $D_{STREAM\ (composite)}$ plays a prominent role to explain the RC might be surprising; a possible explanation lies in the fact that length of instream flow paths is also a metric for runoff storage and exchange within the riparian area, especially in the southern part of the catchment.

For $\Delta_{P/Q,}$ the best model (in terms of AICc) has the two explanatory variables $P_{max\ SOUTH}$ and I_{ASYM} with a R^2 of 0.83 and is considerably better in terms of R^2 than any single predictor model. The best model including a distance metric is $P_{max,All}$ in combination with D_{STREAM} (R^2 0.78), which underlines the prominent role of D_{STREAM} (composite) to explain the hydrologic response in this catchment.

4.4 Measurement network analysis

During the observation period, 23 out of 48 events were captured by the full network of 12 stations, measuring a total amount of rainfall of 120.7 mm. Based on the hydrologic driver analysis, we retain P_{ALL}, $P_{max,ALL}$, I_{ASYM} and D_{STREAM} (composite) as key metrics for the optimal rain gauge network analysis.

Figure 11 shows the best network configurations for 1 to 5 stations and the corresponding RMSE for the select reference metric for the network optimisation (one metric per line).

For a 1-station network, P_{ALL} is best captured when the station is located in the middle of the catchment, while a 2-station network improves substantially the RMSE by arranging the measuring points between the northern and southern parts. Additional stations still improve the RMSE, although to a lesser extent. With a 4-station and 5-station network, the stations tend to align along a north-south transect. For I_{ASYM} and $P_{max,ALL,}$ we see very similar evolution of the spatial patterns as for

https://doi.org/10.5194/hess-2020-371
Preprint. Discussion started: 3 August 2020


Hydrology and Earth System Sciences
Discussions

P_{ALL} for increasing network sizes; for $P_{max,ALL,}$ the RMSE continues however to considerably decrease with the number of stations, which is to be expected for this measure that is more sensitive to spatial-temporal variations of rainfall amount. And for a single station network, the metric I_{ASYM} prefers an station location in the southern part rather than in the northern part.

For D_{STREAM} as a network optimisation metric, the optimal network configuration first selects stations at the extreme ends of the stream network before organizing along a transect as for the other metrics, with one lateral station on the left stream side included in the 5-station network as for $P_{max,ALL}$ (the same) and for I_{ASYM} (a different one).

Considering the small dataset underlying this analysis (23 events), the robustness of the best networks is assessed for two selected metrics (for the P_{ALL} and I_{ASYM}) is evaluated by re-computing the optimal network if between 1 and 3 events are removed from the error computation. Figure 12 shows how frequent a given configuration is identified as being the optimal solution for networks composed of 1 to 3 stations and clearly confirms the optimal solutions found previously.

5 Discussion

5.1 Spatial heterogeneity of rainfall

One of the key identified metrics to characterize the spatial distribution of rainfall, I_{ASYM} splits the catchment into two parts, and averages rainfall observations into two values. Among the records showing a strong rainfall asymmetry, 7 out of the 8 events are too small to cause a detectable streamflow reaction (Figure 7), but one does create a reaction although it only rains over half of the 12 rain gauge stations. Despite of this, the regression analysis based on 14 out of 48 rainfall events suggests that for rainfall events that create a streamflow reaction, the spatial distribution might play an important role for the explanation of the lag time.

The rainfall distance metrics to the stream network (D_{HILLS}) and along the stream network (D_{STREAM}) were designed here to overcome the limitations of the simple asymmetry measure. The prominent role of D_{STREAM} - composite to explain the lag time and RC underlines the importance of characterizing the spatial heterogeneity in terms of geomorphological distances to the actual stream network, which requires more detailed network expansion analyses in future studies.

The fact that D_{STREAM} outperforms here D_{HILLS} for the prediction of RC and lag time is an interesting result: it underlines that even in steep environments, with a priori fast instream processes and limited storage, the riparian area and related subsurface exchange processes could play a more prominent role than what we previously thought. This implies that along-stream processes might need a better representation in rainfall-runoff models, even for small and steep catchments; to date, these processes are often ignored in rainfall-runoff hydrological models at this scale, or are represented with a simple constant velocity transport term (e.g. Schaefli et al., 2014).

5.2 Rain gauge network density

The selected metrics showed the importance and potential of a high density rain gauge network to capture rain events, and to investigate the dynamics of the hydrologic response. The rain gauge network analysis can then be used as a preliminary

https://doi.org/10.5194/hess-2020-371
Preprint. Discussion started: 3 August 2020


Hydrology and Earth System Sciences
Discussions

investigation to implement a permanent network, composed of fewer stations. The reliability of the study is directly dependent on the number of observed rainfall events, i.e. on deployment duration of the rain gauge network. Despite the small size of the catchment, there could potentially be storms that are not or only partially seen by the rain gauge network.

This possibility of missing localized events is highlighted by the event of July 24th (Section 4.1.1), which was considerably underestimated despite of the high density of the deployed network (1 station for 0.9 km² on average, maximal distance of 1,670 m from a point to a rain gauge). The best partial networks composed of 1, 2 or 3 stations (Section 4.4) give for this extremely localized event a total amount of rainfall respectively 12.0 mm, 9.4 mm and 9.2 mm, not far from the 10.6 mm measured with the full network, but these partial networks were trained on the dataset containing the particular event.

With only one station, there is a high risk of totally missing an event, whereas a 2-station network design measuring at least the northern and the southern part of the catchment would i) capture most of the events and ii) give a first estimation of the rainfall spatial distribution.

Overall, the network optimisation analysis with different metrics clearly suggests that to optimally reproduce the hydrologic response in terms of RC and $\Delta_{P/Q}$, we would need to implement at least a three station network in this catchment, organized along a north-south transect, with one of the stations being located in the remote southern part. The north-south organization can be explained by i) the shape of the catchment that also extends longitudinally or ii) a general tendency for rainfall events to move longitudinally, emphasizing the importance, for this case study, to capture spatial configuration of rainfalls over a north-south transect rather than over a west-east transect and iii) the general increasing trend of elevation along this transect.

6 Conclusion

Our analysis of the role of rainfall patterns for the streamflow response is one of the first data-based studies carried out at such a small scale in an Alpine environment. The detailed analysis of 48 events from one summer suggests that spatial rainfall patterns might play a key role to explain the hydrologic response small Alpine catchments. The novelties of the study include the use of a low-cost rain gauge network to capture rainfall patterns, and the design of a new framework to analyze the rainfall-runoff response. The main conclusions from our analysis are:

- A high density rain gauge observation network is a major asset to identify critical areas that are influenced by local rainfall forcing, and give an estimation of the rainfall amount errors made by a partial network.
- A detailed analysis of the hydrological response as a function of rainfall patterns and geomorphology requires a rain gauge network specifically designed for this purpose in conjunction with detailed observations of the stream network expansion before events.
- Such a network should take into account the spatial distribution of distances to the stream network. As shown here, even for small catchments the rainfall distance to the outlet along the stream network might play a key role to explain the hydrologic response. Accordingly, future hydrological modelling studies in small Alpine catchments should investigate the representation of instream transport and storage processes.

https://doi.org/10.5194/hess-2020-371
Preprint. Discussion started: 3 August 2020


Hydrology and Earth System Sciences
Discussions

The analysis framework developed here is readily transferable to other settings. Given the low cost of the deployed rainfall sensor network, the approach has potential for future detailed studies in to-date sparsely gauged catchments.

445

450

455

460 *Data availability.* Rainfall and streamflow data used for this paper, and the MatLab code written to visualize the data are available at https://doi.org/10.5281/zenodo.3946242.

Author contributions. AM and BS conceived the ideas and designed methodology; AM, LB and HB collected the rainfall data; AM and LB analyzed the data; AM and BS led the writing of the manuscript. All authors contributed critically to the drafts
465 and gave final approval for publication.

Competing interests. Author BS is a member of the editorial board of the journal, but otherwise there are no competing interests present that the authors are aware of.

470 *Acknowledgements.* The work of the authors is funded by the Swiss National Science Foundation (SNSF), grant number PP00P2_157611.

https://doi.org/10.5194/hess-2020-371
Preprint. Discussion started: 3 August 2020

Hydrology and Earth System Sciences
Discussions

Appendix A: Drop-counting rain gauge calibration and data correction

Technical characteristics of the Pluvimate drop-counting rain gauges (see Section 3.1) are detailed in Benoit et al. (2018a); for this study we extended the experimental tests to intensities up to 150 mm/h. It appears that for intensities up to 20 mm/h (99.88 % of the measured 2-min intensities during the 2018 observation period, see Figure A1) the linear relationship between drop count and rain intensity gives a good estimate (uncertainty below 5 %); beyond 20 mm/h the linear relationship underestimates the rainfall intensities, to reach 10 % of error at 60 mm/h and 15 % at 150 mm/h (Figure A1). For this study, rainfall intensities over 20 mm/h are corrected using a polynomial law based on the experimental measures.

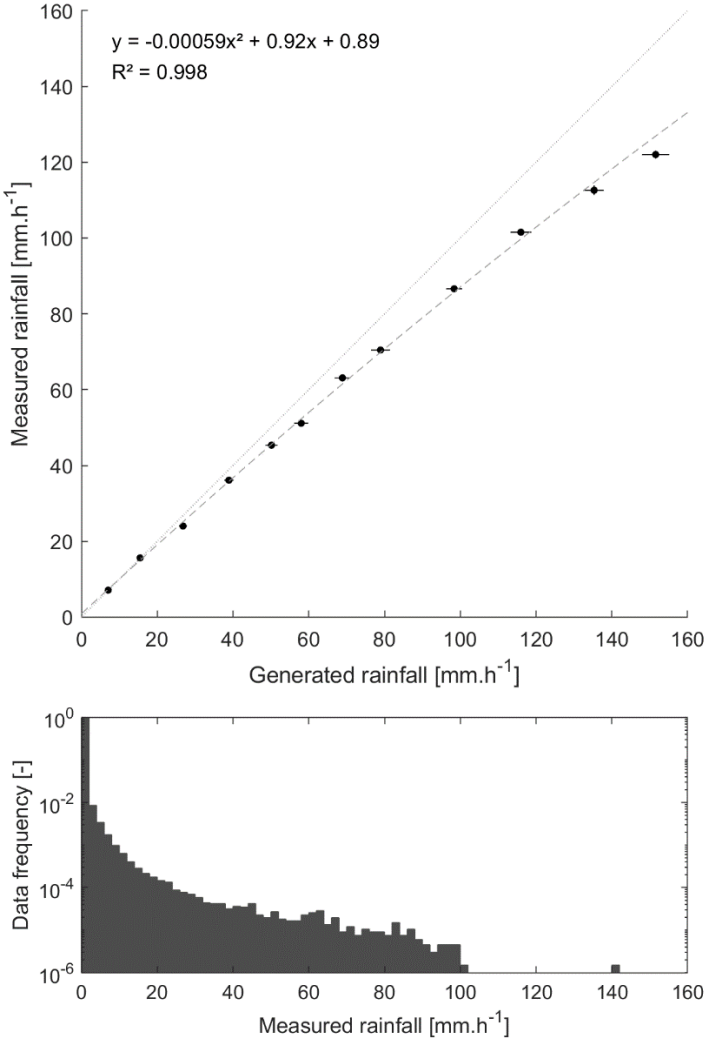

Figure A1. Calibration curve (on top) of the Pluvimate rain gauges based on experimental measures with controlled rainfall input, and (at the bottom) the data frequency measured in situ.

https://doi.org/10.5194/hess-2020-371
Preprint. Discussion started: 3 August 2020

References

Akaike, H.: A new look at the statistical model identification, IEEE Transactions on Automatic Control, 19, 716-723, 10.1109/TAC.1974.1100705, 1974.

Bardossy, A., and Das, T.: Influence of rainfall observation network on model calibration and application, Hydrol Earth Syst Sc, 12, 77-89, DOI 10.5194/hess-12-77-2008, 2008.

Bell, V. A., and Moore, R. J.: The sensitivity of catchment runoff models to rainfall data at different spatial scales, Hydrol Earth Syst Sc, 4, 653-667, DOI 10.5194/hess-4-653-2000, 2000.

Benoit, L., Allard, D., and Mariethoz, G.: Stochastic Rainfall Modeling at Sub-kilometer Scale, Water Resour Res, 54, 4108-4130, 10.1029/2018WR022817, 2018a.

Benoit, L., Vrac, M., and Mariethoz, G.: Dealing with non-stationarity in sub-daily stochastic rainfall models, Hydrol. Earth Syst. Sci., 22, 5919-5933, 10.5194/hess-22-5919-2018, 2018b.

Berne, A., and Krajewski, W. F.: Radar for hydrology: Unfulfilled promise or unrecognized potential?, Adv Water Resour, 51, 357-366, 10.1016/j.advwatres.2012.05.005, 2013.

Blume, T., Zehe, E., and Bronstert, A.: Rainfall-runoff response, event-based runoff coefficients and hydrograph separation, Hydrol. Sci. J.-J. Sci. Hydrol., 52, 843-862, 10.1623/hysj.52.5.843, 2007.

Bras, R. L., and Rodriguez-Iturbe, I.: Network design for estimation of areal mean of rainfall events, Water Resour Res, 12, 1185-1195, 10.1029/WR012i006p01185, 1976a.

Bras, R. L., and Rodriguez-Iturbe, I.: Rainfall network design for runoff prediction, Water Resour Res, 12, 1197-1208, 10.1029/WR012i006p01197, 1976b.

Burnham, K. P., Anderson, D. R., and Huyvaert, K. P.: AIC model selection and multimodel inference in behavioral ecology: some background, observations, and comparisons, Behav Ecol Sociobiol, 65, 23-35, 10.1007/s00265-010-1029-6, 2011.

Ceperley, N., Michelon, A., Escoffier, N., Mayoraz, G., Boix Canadell, M., Horgby, A., Hammer, F., Antoniazza, G., Schaefli, B., Lane, S. N., Rickenmann, D., and Boss, S.: Salt gauging and stage-discharge curve, Avançon de Nant, outlet Vallon de Nant catchment, Zenodo, 10.5281/zenodo.1154798, 2018.

Chacon-Hurtado, J. C., Alfonso, L., and Solomatine, D. P.: Rainfall and streamflow sensor network design: a review of applications, classification, and a proposed framework, Hydrol Earth Syst Sc, 21, 3071-3091, 10.5194/hess-21-3071-2017, 2017.

Cherix, D., and Vittoz, P.: Synthèse et conclusions aux Journées de la biodiversité 2008 dans le Vallon de Nant, Biodiversité du Vallon de Nant. Mémoire de la Société vaudoise des Sciences naturelles, 23, 225-240, 2009.

https://doi.org/10.5194/hess-2020-371
Preprint. Discussion started: 3 August 2020


Hydrology and Earth System Sciences
Discussions

Foehn, A., García Hernández, J., Schaefli, B., and De Cesare, G.: Spatial interpolation of precipitation from multiple rain gauge networks and weather radar data for operational applications in Alpine catchments, Journal of Hydrology, 563, 1092-1110, 10.1016/j.jhydrol.2018.05.027, 2018a.

Foehn, A., Hernandez, J. G., Schaefli, B., and De Cesare, G.: Spatial interpolation of precipitation from multiple rain gauge networks and weather radar data for operational applications in Alpine catchments, Journal of Hydrology, 563, 1092-1110, 2018b.

Germann, U., Galli, G., Boscacci, M., and Bolliger, M.: Radar precipitation measurement in a mountainous region, Q J Roy Meteor Soc, 132, 1669-1692, 10.1256/qj.05.190, 2006.

Germann, U., Boscacci, M., Gabella, M., and Sartori, M.: Peak Performance: Radar design for prediction in the Swiss Alps, Meteorological Technology International, 42-45, 2015.

Gharari, S., Hrachowitz, M., Fenicia, F., and Savenije, H. H. G.: Hydrological landscape classification: investigating the performance of HAND based landscape classifications in a central European meso-scale catchment, Hydrol Earth Syst Sc, 15, 3275-3291, 10.5194/hess-15-3275-2011, 2011.

Grand, S., Rubin, A., Verrecchia, E. P., and Vittoz, P.: Variation in Soil Respiration across Soil and Vegetation Types in an Alpine Valley, Plos One, 11, ARTN e0163968, 10.1371/journal.pone.0163968, 2016.

Guastini, E., Zuecco, G., Errico, A., Castelli, G., Bresci, E., Preti, F., and Penna, D.: How does streamflow response vary with spatial scale? Analysis of controls in three nested Alpine catchments, J Hydrol, 570, 705-718, 10.1016/j.jhydrol.2019.01.022, 2019.

Henn, B., Newman, A. J., Livneh, B., Daly, C., and Lundquist, J. D.: An assessment of differences in gridded precipitation datasets in complex terrain, J Hydrol, 556, 1205-1219, 10.1016/j.jhydrol.2017.03.008, 2018.

Horgby, A., Canadell, M. B., Utseth, A. J., Vennemann, T. W., and Battin, T. J.: High-Resolution Spatial Sampling Identifies Groundwater as Driver of CO2 Dynamics in an Alpine Stream Network, J Geophys Res-Biogeo, 124, 1961-1976, 10.1029/2019jg005047, 2019.

Horgby, A. L. V.: Spatiotemporal Drivers of CO2 Dynamics and Evasion Fluxes from Mountain Streams, 85, 10.5075/epfl-thesis-7583, 2019.

Lane, S. N., Borgeaud, L., and Vittoz, P.: Emergent geomorphic-vegetation interactions on a subalpine alluvial fan, Earth Surf Proc Land, 41, 72-86, 10.1002/esp.3833, 2016.

Lobligeois, F., Andreassian, V., Perrin, C., Tabary, P., and Loumagne, C.: When does higher spatial resolution rainfall information improve streamflow simulation? An evaluation using 3620 flood events, Hydrology and Earth System Sciences, 18, 575-594, 10.5194/hess-18-575-2014, 2014.

Mei, Y. W., Anagnostou, E. N., Stampoulis, D., Nikolopoulos, E. I., Borga, M., and Vegara, H. J.: Rainfall organization control on the flood response of mild-slope basins, Journal of Hydrology, 510, 565-577, 10.1016/j.jhydrol.2013.12.013, 2014.

https://doi.org/10.5194/hess-2020-371
Preprint. Discussion started: 3 August 2020

Michelon, A., Schaefli, B., Ceperley, N., and Beria, H.: Weather dataset from Vallon de Nant, Switzerland, until July 2017, Zenodo, 10.5281/zenodo.1042473, 2017.

Moulin, L., Gaume, E., and Obled, C.: Uncertainties on mean areal precipitation: assessment and impact on streamflow simulations, Hydrol Earth Syst Sc, 13, 99-114, DOI 10.5194/hess-13-99-2009, 2009.

Nicótina, L., Alessi Celegon, E., Rinaldo, A., and Marani, M.: On the impact of rainfall patterns on the hydrologic response, Water Resour Res, 44, W12401, 10.1029/2007WR006654, 2008.

Nikolopoulos, E. I., Anagnostou, E. N., Borga, M., Vivoni, E. R., and Papadopoulos, A.: Sensitivity of a mountain basin flash flood to initial wetness condition and rainfall variability, J Hydrol, 402, 165-178, 10.1016/j.jhydrol.2010.12.020, 2011.

Nobre, A. D., Cuartas, L. A., Hodnett, M., Renno, C. D., Rodrigues, G., Silveira, A., Waterloo, M., and Saleska, S.: Height Above the Nearest Drainage - a hydrologically relevant new terrain model, J Hydrol, 404, 13-29, 10.1016/j.jhydrol.2011.03.051, 2011.

Obled, C., Wendling, J., and Beven, K.: The sensitivity of hydrological models to spatial rainfall patterns - an evaluation using observed data, Journal of Hydrology, 159, 305-333, 1994.

Pechlivanidis, I. G., McIntyre, N., and Wheater, H. S.: The significance of spatial variability of rainfall on simulated runoff: an evaluation based on the Upper Lee catchment, UK, Hydrol. Res., 48, 1118-1130, 10.2166/nh.2016.038, 2017.

Penna, D., Tromp-van Meerveld, H. J., Gobbi, A., Borga, M., and Dalla Fontana, G.: The influence of soil moisture on threshold runoff generation processes in an alpine headwater catchment, Hydrol Earth Syst Sc, 15, 689-702, 10.5194/hess-15-689-2011, 2011.

Renno, C. D., Nobre, A. D., Cuartas, L. A., Soares, J. V., Hodnett, M. G., Tomasella, J., and Waterloo, M. J.: HAND, a new terrain descriptor using SRTM-DEM: Mapping terra-firme rainforest environments in Amazonia, Remote Sens Environ, 112, 3469-3481, 10.1016/j.rse.2008.03.018, 2008.

Rinaldo, A., Marani, M., and Rigon, R.: Geomorphological dispersion, Water Resour Res, 27, 513-525, 1991.

Rinaldo, A., Banavar, J. R., and Maritan, A.: Trees, networks, and hydrology Water Resour Res, 42, W06D07 10.1029/2005WR004108, 2006a.

Rinaldo, A., Botter, G., Bertuzzo, E., Uccelli, A., Settin, T., and Marani, M.: Transport at basin scales: 1. Theoretical framework, Hydrol Earth Syst Sc, 10, 19-29, DOI 10.5194/hess-10-19-2006, 2006b.

Rodriguez-Blanco, M. L., Taboada-Castro, M. M., and Taboada-Castro, M. T.: Rainfall-runoff response and event-based runoff coefficients in a humid area (northwest Spain), Hydrolog Sci J, 57, 445-459, 10.1080/02626667.2012.666351, 2012.

Ross, C. A., Ali, G., Spence, C., Oswald, C., and Casson, N.: Comparison of event-specific rainfall-runoff responses and their controls in contrasting geographic areas, Hydrol Process, 33, 1961-1979, 10.1002/hyp.13460, 2019.

https://doi.org/10.5194/hess-2020-371
Preprint. Discussion started: 3 August 2020

575 Rowley, M. C., Grand, S., and Verrecchia, É. P. J. B.: Calcium-mediated stabilisation of soil organic carbon, 137, 27-49, 10.1007/s10533-017-0410-1, 2018.

Schaefli, B., Nicotina, L., Imfeld, C., Da Ronco, P., Bertuzzo, E., and Rinaldo, A.: SEHR-ECHO v1.0: a Spatially Explicit Hydrologic Response model for ecohydrologic applications, Geosci Model Dev, 7, 2733-2746, 2014.

Shah, S. M. S., Oconnell, P. E., and Hosking, J. R. M.: Modelling the effects of spatial variability in rainfall on catchment
580 response .1. Formulation and calibration of a stochastic rainfall field model, Journal of Hydrology, 175, 67-88, 10.1016/s0022-1694(96)80006-0, 1996.

Sideris, I. V., Gabella, M., Erdin, R., and Germann, U.: Real-time radar-rain-gauge merging using spatio-temporal co-kriging with external drift in the alpine terrain of Switzerland, Q J Roy Meteor Soc, 140, 1097-1111, 10.1002/qj.2188, 2014.

Singh, V. P.: Effect of spatial and temporal variability in rainfall and watershed characteristics on stream flow hydrograph,
585 Hydrol Process, 11, 1649-1669, 1997.

St-Hilaire, A., Ouarda, T., Lachance, M., Bobee, B., Gaudet, J., and Gignac, C.: Assessment of the impact of meteorological network density on the estimation of basin precipitation and runoff: a case study, Hydrological Processes, 17, 3561-3580, 10.1002/hyp.1350, 2003.

Stisen, S., and Sandholt, I.: Evaluation of remote-sensing-based rainfall products through predictive capability in hydrological
590 runoff modelling, Hydrol Process, 24, 879-891, 10.1002/hyp.7529, 2010.

swissALTI3D: The digital elevation model of Switzerland, 2012.

Tarboton, D. G., Bras, R. L., and Puente, C. E.: Combined hydrologic sampling criteria for rainfall and streamflow, Journal of Hydrology, 95, 323-339, https://doi.org/10.1016/0022-1694(87)90009-6, 1987.

Tetzlaff, D., and Uhlenbrook, S.: Significance of spatial variability in precipitation for process-oriented modelling: results
595 from two nested catchments using radar and ground station data, Hydrol Earth Syst Sc, 9, 29-41, DOI 10.5194/hess-9-29-2005, 2005.

Thornton, J. M., Mariethoz, G., and Brunner, P.: A 3D geological model of a structurally complex Alpine region as a basis for interdisciplinary research, Scientific Data, 5, 180238, 10.1038/sdata.2018.238

Tromp-van Meerveld, H. J., and McDonnell, J. J.: Threshold relations in subsurface stormflow: 2. The fill and spill hypothesis,
600 Water Resour Res, 42, Artn W02411, 10.1029/2004wr003800, 2006.

Viglione, A., Chirico, G. B., Woods, R., and Bloschl, G.: Generalised synthesis of space-time variability in flood response. An analytical framework, Journal of Hydrology, 394, 198-212, 10.1016/j.jhydrol.2010.05.047, 2010.

Volpi, E., Di Lazzaro, M., and Fiori, A.: A simplified framework for assessing the impact of rainfall spatial variability on the hydrologic response, Advances in Water Resources, 46, 1-10, https://doi.org/10.1016/j.advwatres.2012.04.011, 2012.

https://doi.org/10.5194/hess-2020-371
Preprint. Discussion started: 3 August 2020


Hydrology and Earth System Sciences
Discussions

605 Woods, R., and Sivapalan, M.: A synthesis of space-time variability in storm response: rainfall, runoff generation, and routing, Water Resour Res, 35, 2469-2485, 1999.

Xu, H. L., Xu, C. Y., Chen, H., Zhang, Z. X., and Li, L.: Assessing the influence of rain gauge density and distribution on hydrological model performance in a humid region of China, Journal of Hydrology, 505, 1-12, 10.1016/j.jhydrol.2013.09.004, 2013.

610 Zehe, E., Becker, R., Bardossy, A., and Plate, E.: Uncertainty of simulated catchment runoff response in the presence of threshold processes: Role of initial soil moisture and precipitation, J Hydrol, 315, 183-202, 10.1016/j.jhydrol.2005.03.038, 2005.

Zillgens, B., Merz, B., Kirnbauer, R., and Tilch, N.: Analysis of the runoff response of an alpine catchment at different scales, Hydrol Earth Syst Sc, 11, 1441-1454, DOI 10.5194/hess-11-1441-2007, 2007.

615 Zoccatelli, D., Borga, M., Chirico, G. B., and Nikolopoulos, E. I.: The relative role of hillslope and river network routing in the hydrologic response to spatially variable rainfall fields, Journal of Hydrology, 531, 349-359, 10.1016/j.jhydrol.2015.08.014, 2015.

https://doi.org/10.5194/hess-2020-371
Preprint. Discussion started: 3 August 2020

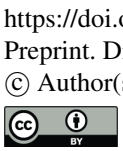

Hydrology and Earth System Sciences
Discussions
Open Access
EGU

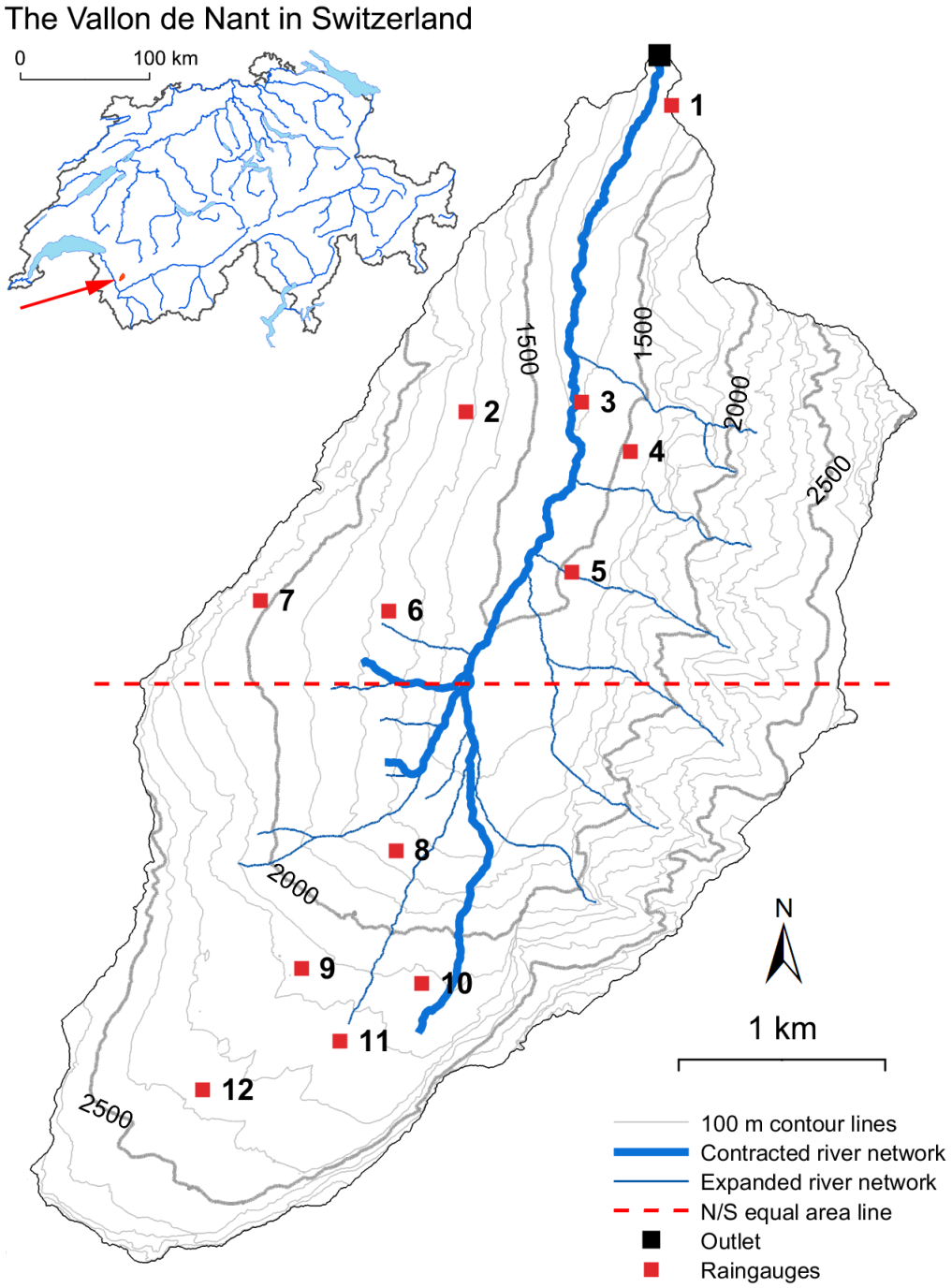

620

Figure 1. Map of the Vallon de Nant and location of the 12 rain gauges. The streamflow is measured on the main river at the outlet (46.25301 N / 7.10954 E in WGS84 coordinates). The red dashed line splits the catchment area into two parts of equal area.

https://doi.org/10.5194/hess-2020-371
Preprint. Discussion started: 3 August 2020

Hydrology and Earth System Sciences
Discussions
Open Access
EGU

Figure 2. River stage measure at the outlet. The streamflow is here measured between 0.96 and 1.13 $m^3.s^{-1}$.

https://doi.org/10.5194/hess-2020-371
Preprint. Discussion started: 3 August 2020

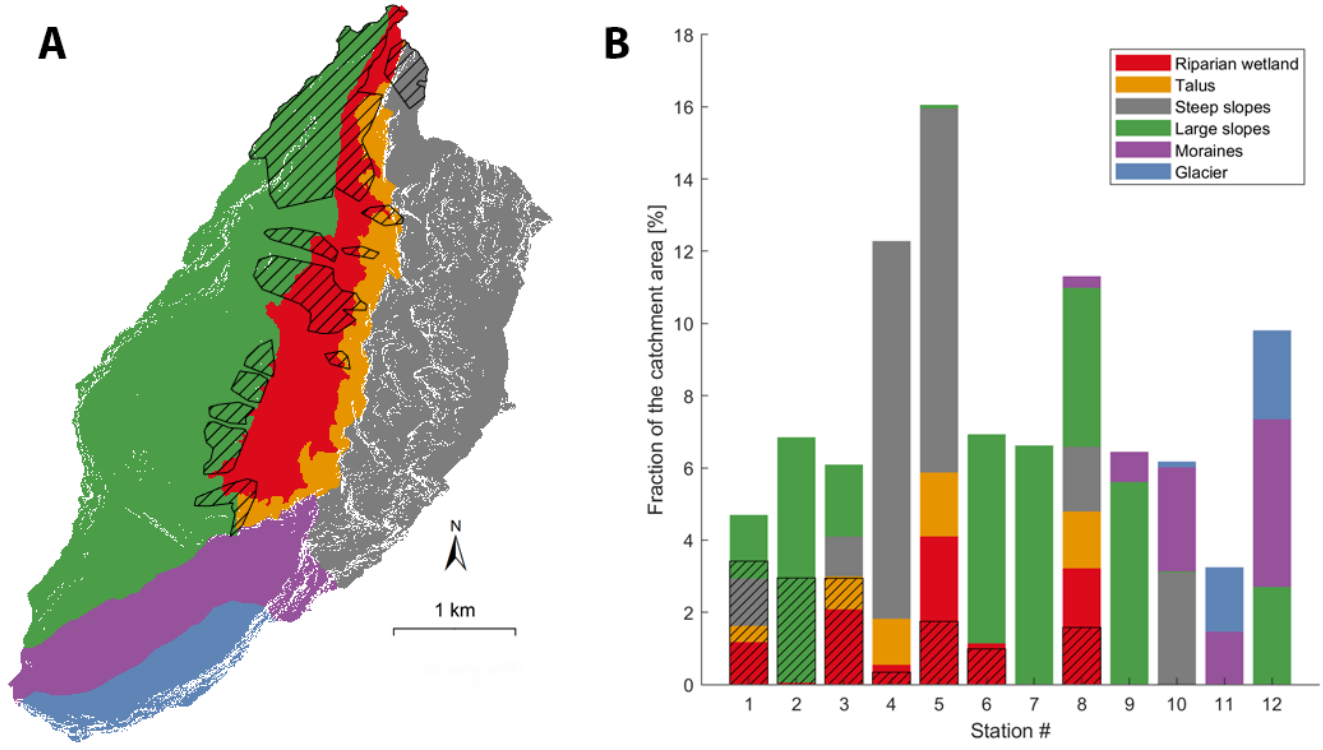

Figure 3. Hydrological units in the Vallon de Nant (left) and their relative areas within the spatial imprint attributed to each rain gauge (right). The hatched area corresponds to the densely forested area.

https://doi.org/10.5194/hess-2020-371
Preprint. Discussion started: 3 August 2020

Hydrology and Earth System Sciences
Discussions
Open Access
EGU

640 Figure 4. Drop-counting rain gauge used for rainfall measures. The Pluvimate is set-up vertically between 0.8 and 1.2 meters above the ground level (a). A tip at the end of the funnel (b) creates a calibrated drop of water that falls on the sensor, (c) which counts and records the number of drops during a given amount of time.

https://doi.org/10.5194/hess-2020-371
Preprint. Discussion started: 3 August 2020

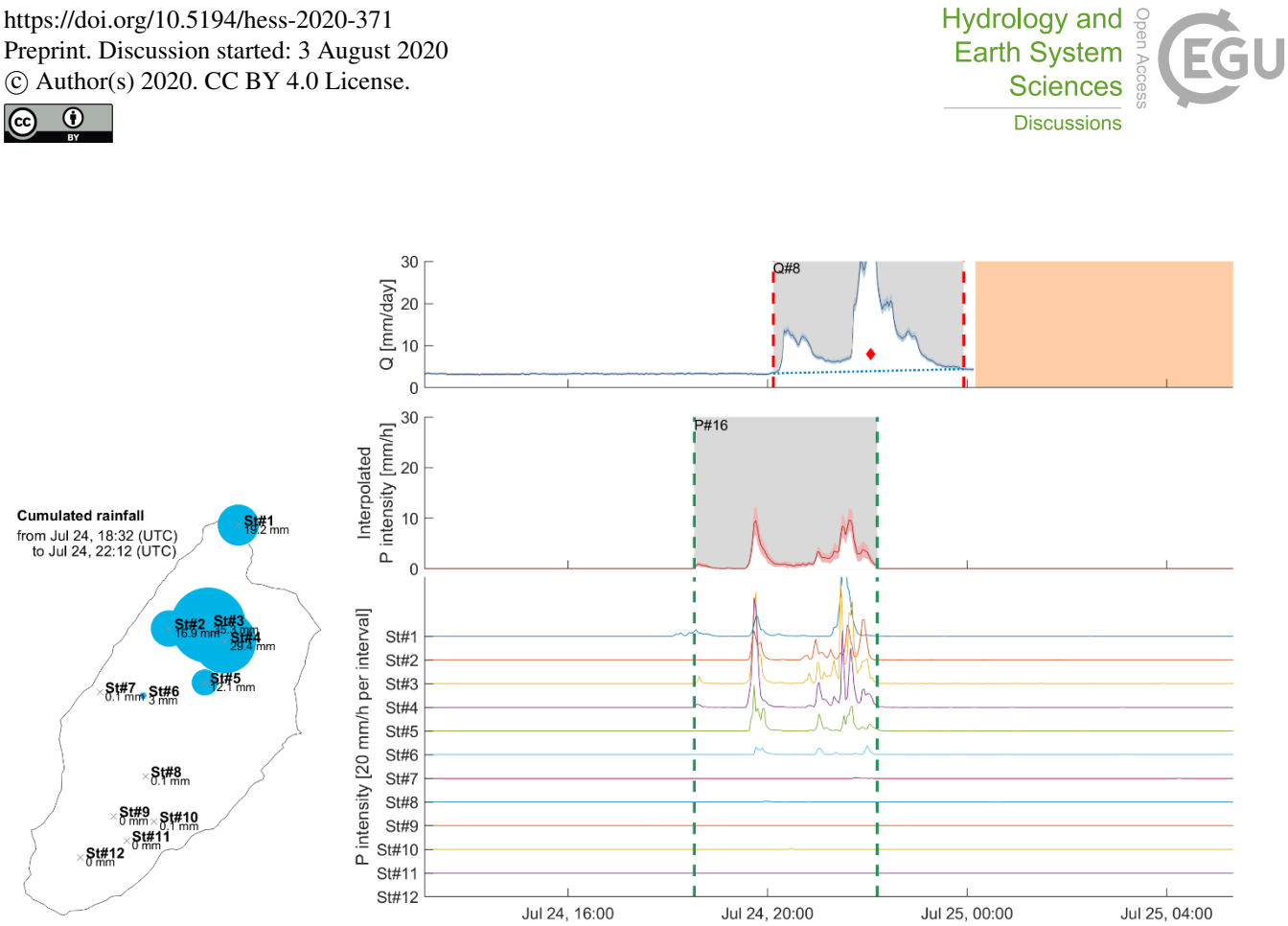

645 Figure 5. Summary of the recorded rainfall and streamflow for the rainfall event of July 24th 2018 at 6:32 PM (UTC).

https://doi.org/10.5194/hess-2020-371
Preprint. Discussion started: 3 August 2020

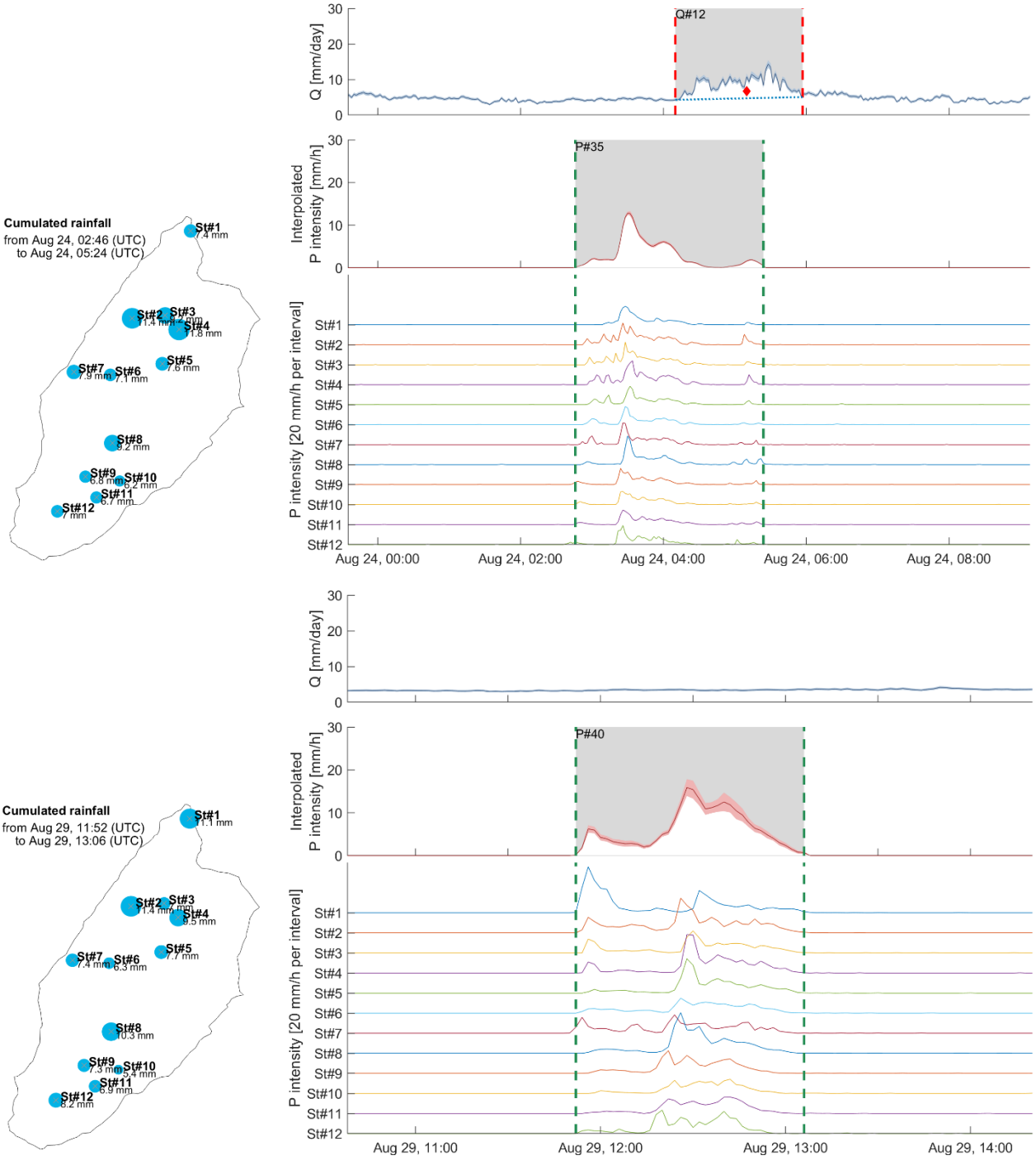

Figure 6. Summary of the recorded rainfall and streamflow for the rainfall events of August 24th 2018 at 2:46 AM (top) and August 29th 2018 at 11:52 AM (bottom).

https://doi.org/10.5194/hess-2020-371
Preprint. Discussion started: 3 August 2020

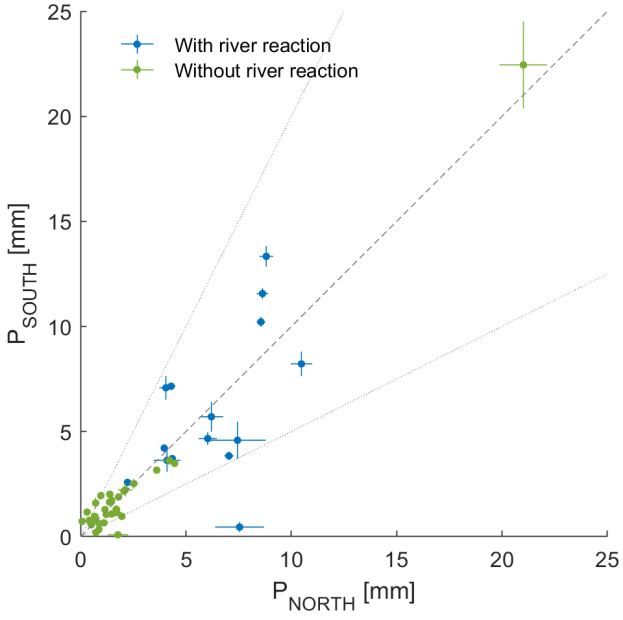

Figure 7. Scatterplot of the rainfall amounts over the northern and the southern parts of the catchment for all 48 rainfall events. The dotted lines show the 1/2 and 2/1 lines which correspond to twice more rainfall in one part of the catchment than in the other or to $|I_{ASYM}| > 0.33$. The outlier (event of 6-Aug with 43.5 mm of rainfall in total) is flagged without river reaction as the river stage measure was disturbed during this period.

https://doi.org/10.5194/hess-2020-371
Preprint. Discussion started: 3 August 2020

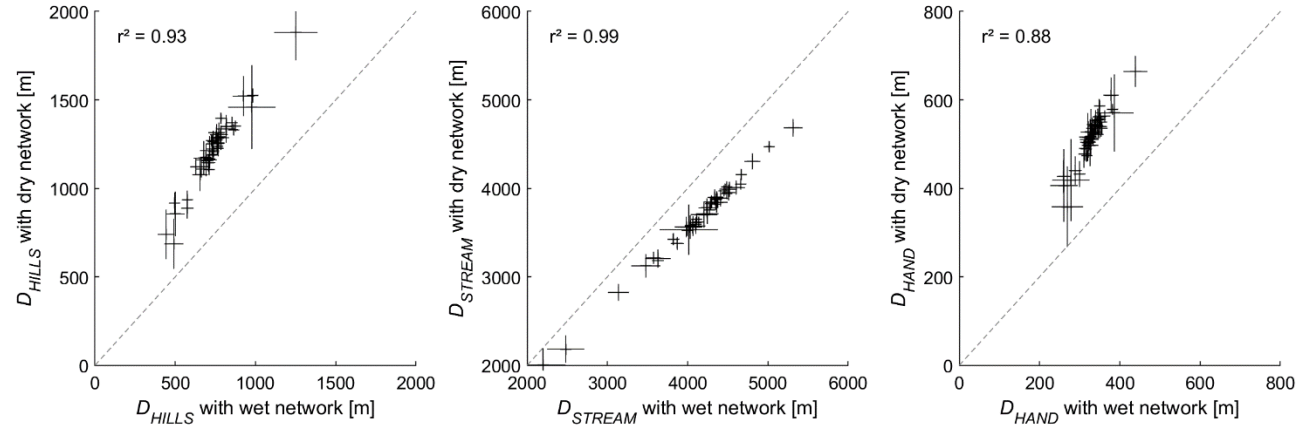

Figure 8. Scatterplots of the distance metrics for the dry network state versus the wet state, for all 48 rainfall events. The bars indicate the standard deviation obtained from the 20 rainfall field realisations. r^2 indicates the linear correlation.

https://doi.org/10.5194/hess-2020-371
Preprint. Discussion started: 3 August 2020

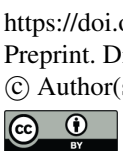

Hydrology and Earth System Sciences
Discussions
Open Access
EGU

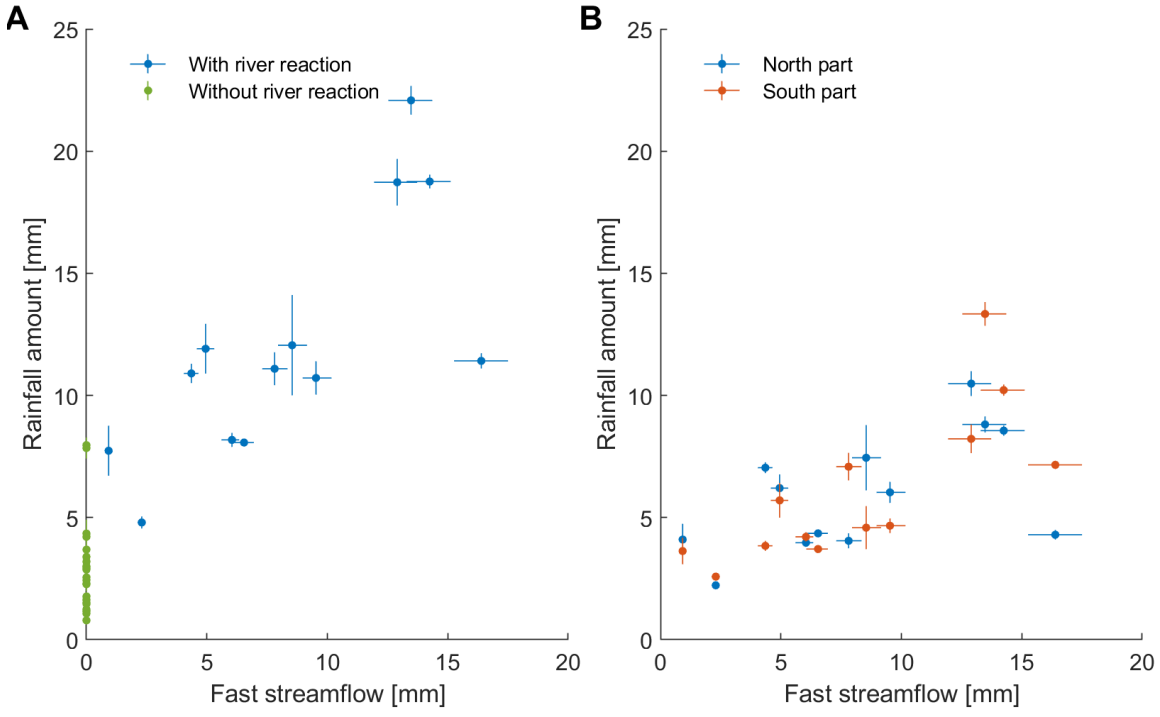

Figure 9. A) Rainfall amounts against fast streamflow, separating the northern and southern parts of the catchment (for separation line, see Figure 1); events without reaction are not shown. The events 24 July (P_{ALL}=8.0 mm, Q_{FAST} = 30.4 mm and of 6 Aug (P_{ALL}=43.5 mm, Q not recorded) are out of the axis. B) total rainfall amounts against fast streamflow, highlighting the threshold for streamflow reaction. The bars show the standard deviation of estimated rainfall (Section 3.2) and of streamflow (Section 2).

https://doi.org/10.5194/hess-2020-371
Preprint. Discussion started: 3 August 2020

Hydrology and Earth System Sciences
Discussions
Open Access
EGU

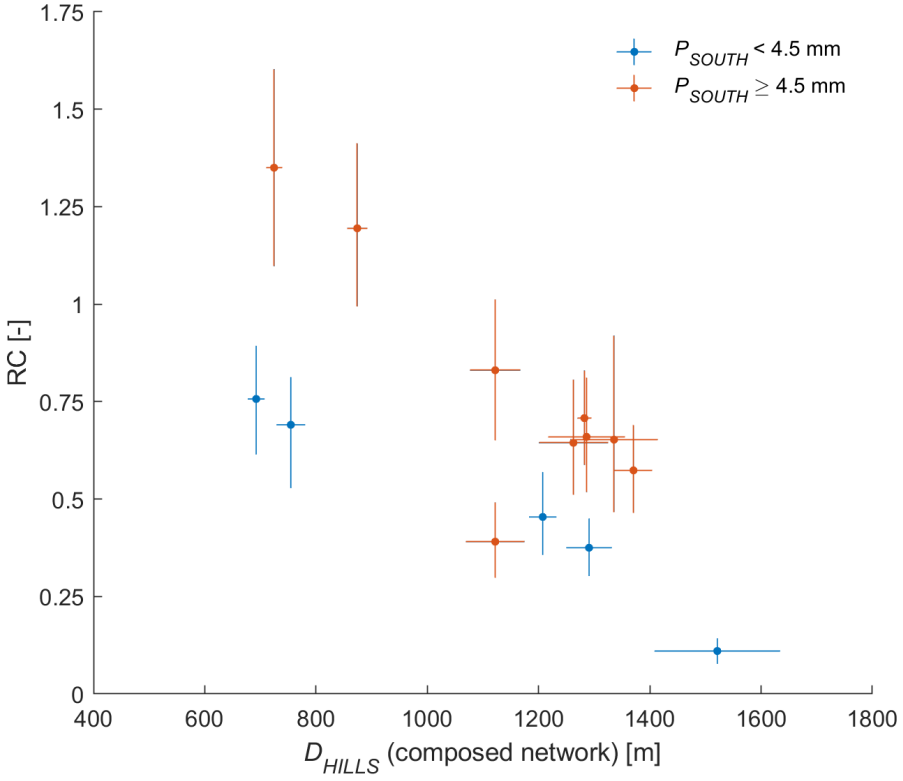

Figure 10. Runoff coefficient against D_{HILLS}, highlighting events with high rainfall amounts in the southern part, i.e. events with P_{SOUTH}>4.5 mm, the 24 July event with 3.02 <RC<4.85 and D_{HILLS}=740±140 m has been discarded (see Section 4.1.1).

https://doi.org/10.5194/hess-2020-371
Preprint. Discussion started: 3 August 2020

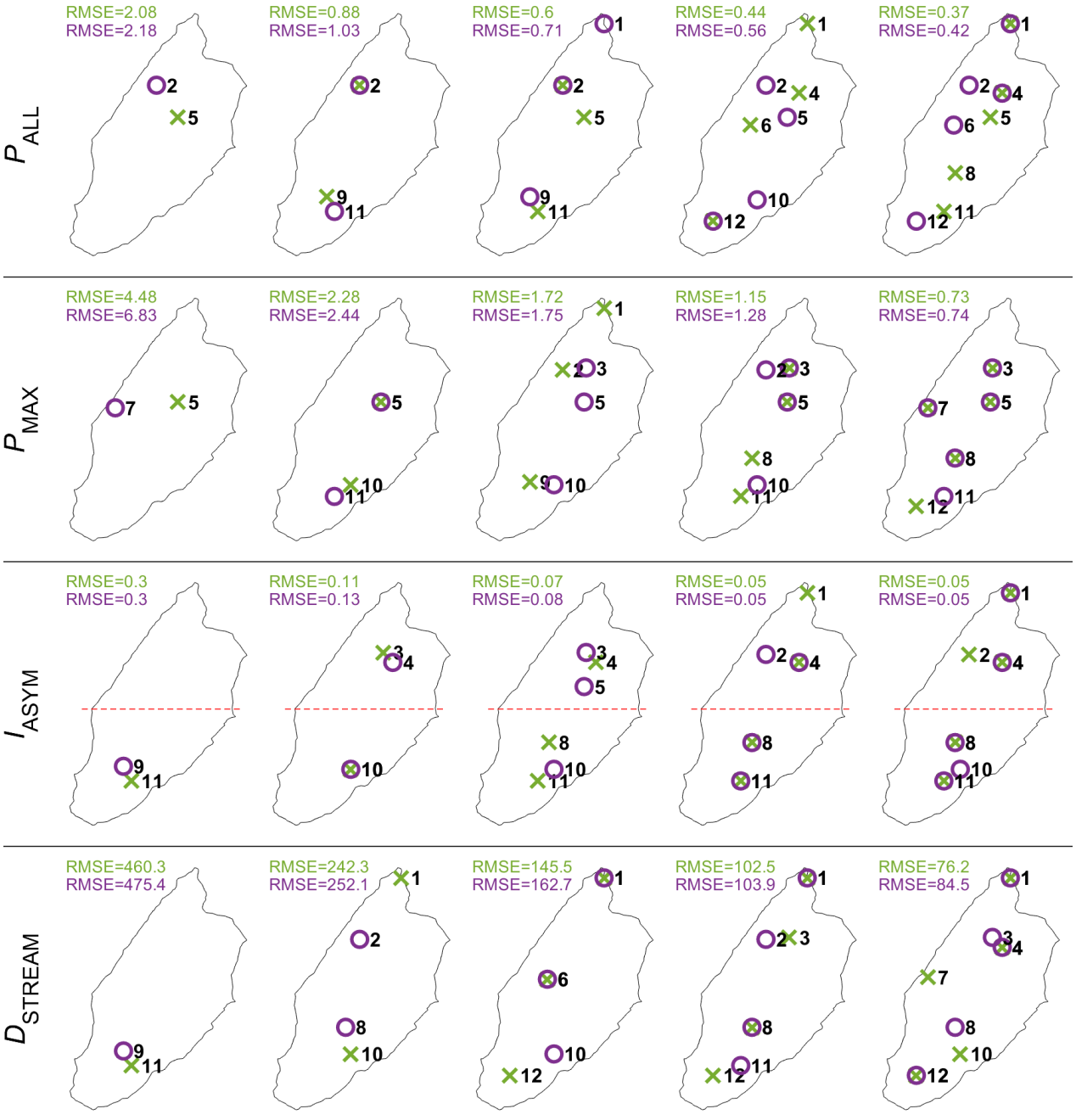

Figure 11. First (green) and second (purple) best networks and associated RMSE values for 1 to 5 stations resulting from the minimization of the RMSE over 23 events for the P_{ALL}, P_{MAX}, I_{ASYM} and D_{STREAM}. The red dashed line splits the catchments into two parts of equal area.

https://doi.org/10.5194/hess-2020-371
Preprint. Discussion started: 3 August 2020

Hydrology and Earth System Sciences
Discussions
Open Access
EGU

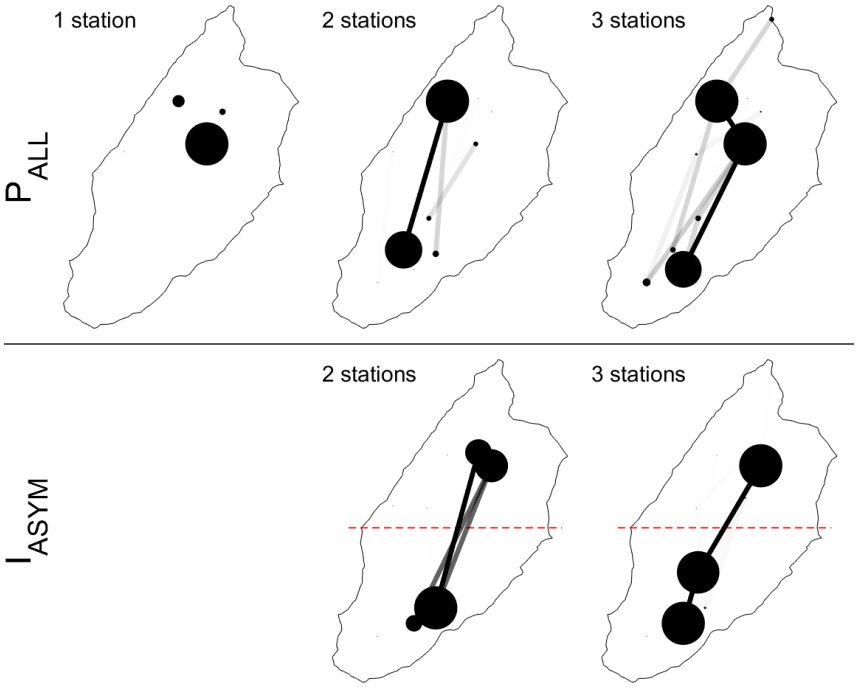

695

Figure 12. Sensitivity test over the best network from 1 to 3 station, evaluated by removing from 1 to 3 events over the 23 events (2047 combinations) for the P_{ALL} and I_{ASYM}. The result is presented graphically: larger dots and wider links represent configurations that are found more frequently than others over the different altered simulations. The red dashed line splits the catchments into two parts of equal area.

700

https://doi.org/10.5194/hess-2020-371
Preprint. Discussion started: 3 August 2020

Hydrology and Earth System Sciences
Discussions

Table 1. List and definition of the metrics used in this study, with corresponding parameter name or abbreviation used in the text.

Description	Notation, Unit
Rainfall interpolated over entire catchment	P_{ALL}, mm
Rainfall interpolated over north half of catchment	P_{NORTH}, mm
Rainfall interpolated over south half of catchment	P_{SOUTH}, mm
Rainfall event duration	$P_{DURATION}$, min
River reaction event duration	$Q_{DURATION}$, min
Index of spatial asymmetry of rainfall	I_{ASYM}, -
Mean distance of rainfall spatial center of mass to stream network (along hillslopes)	D_{HILLS}, m
Mean distance of rainfall spatial center of mass to outlet along the stream network	D_{STREAM}, m
Mean height above the nearest drainage	D_{HAND}, m
Cumulated amount of rainfall for the last X days	$W_{X\ days}$, mm
Streamflow at the start of the streamflow event	Q_{INIT}, mm
Fast streamflow amount	Q_{FAST}, mm
Rainfall runoff coefficient	RC, -
Lag time between the first third of cumulated rainfall and the first third of cumulated river quickflow	$\Delta_{P/Q}$, min

https://doi.org/10.5194/hess-2020-371
Preprint. Discussion started: 3 August 2020

Hydrology and Earth System Sciences
Discussions
Open Access
EGU

Table 2. List of recorded precipitation events with streamflow reaction. Full details are available in the Supplementary Material.

Date	$P_{DURATION}$ [min]	$Q_{DURATION}$ [min]	$\Delta_{P/Q}$ [min]	P_{ALL} [mm]	P_{NORTH} [mm]	P_{SOUTH} [mm]	$W_{3\ days}$ [mm]	Q_{INIT} [mm]	Q_{FAST} [mm]	RC [-]	I_{ASYM} [-]	D_{HILLS} [m]	D_{STREAM} [m]	D_{HAND} [m]
2-Jul-18	42	44	24	7.7	4.1	3.6	3.2	7.9	0.9	0.12	-0.06	1521	4008	611
3-Jul-18	40	135	23	12.1	7.4	4.6	12.7	7.5	8.5	0.71	-0.24	1336	3842	550
5-Jul-18	224	309	71	8.2	4.0	4.2	29.8	6.0	6.0	0.74	0.03	755	4374	350
6-Jul-18	478	587	65	20.2	8.6	11.6	40.3	5.8	25.9	1.29	0.15	874	4450	355
14-Jul-18	358	302	49	18.7	10.5	8.2	0.0	4.5	12.9	0.69	-0.12	1263	3574	554
15-Jul-18	136	281	33	10.7	6.0	4.7	18.9	5.5	9.5	0.89	-0.13	1122	3377	528
20-Jul-18	288	228	49	18.8	8.6	10.2	3.4	4.8	14.2	0.76	0.09	1282	3823	541
24-Jul-18	220	229	45	8.0	7.5	0.5	12.2	3.1	30.4	3.78	0.02	740	2184	419
14-Aug-18	204	152	47	11.1	4	7.1	10.2	4.0	7.8	0.70	0.27	1286	4305	540
17-Aug-18	152	109	38	11.9	6.2	5.7	17.5	3.2	4.9	0.42	-0.04	1122	3780	490
23-Aug-18	388	237	47	22.1	8.8	13.3	5.4	2.4	13.5	0.61	0.20	1371	3756	563
24-Aug-18	158	107	40	8.1	4.4	3.7	29.5	4.1	6.5	0.81	-0.08	692	4114	320
29-Aug-18	72	116	48	4.8	2.2	2.6	12.4	3.0	2.3	0.48	0.07	1207	3526	524
01-sept-18	628	341	101	11.4	4.3	7.2	20.4	3.4	16.4	1.44	0.25	725	4487	331
13-sept-18	370	59	45	10.9	7.0	3.8	0.0	2.6	4.4	0.40	-0.29	1291	3594	556

https://doi.org/10.5194/hess-2020-371
Preprint. Discussion started: 3 August 2020

Hydrology and Earth System Sciences
Discussions

Table 3. Correlations between rainfall amounts, asymmetry metrics and hydrologic response metrics for the 14 events with streamflow reaction (after discarding the 24 July event). Absolute values equal or over 0.60 are in bold.

	P_{ALL} [mm]	P_{NORTH} [mm]	P_{SOUTH} [mm]	$P_{max\ ALL}$ [mm.h^{-1}]	$P_{max\ NORTH}$ [mm.h^{-1}]	$P_{max\ SOUTH}$ [mm.h^{-1}]	I_{ASYM} [-]	$W_{3\ days}$ [mm]	Q_{INIT} [mm]	Q_{FAST} [mm]	$P_{DURATION}$ [min]	$Q_{DURATION}$ [min]	$\Delta_{P/Q}$ [min]
P_{ALL} [mm]	-												
P_{NORTH} [mm]	**0.89**	-											
P_{SOUTH} [mm]	**0.94**	**0.69**	-										
$P_{max\ ALL}$ [mm.h^{-1}]	0.01	0.19	-0.12	-									
$P_{max\ NORTH}$ [mm.h^{-1}]	0.09	0.33	-0.11	**0.96**	-								
$P_{max\ SOUTH}$ [mm.h^{-1}]	0.19	0.19	0.16	**0.87**	**0.78**	-							
I_{ASYM} [-]	0.25	-0.20	0.55	-0.42	-0.56	-0.06	-						
$W_{3\ days}$ [mm]	-0.19	-0.30	-0.09	-0.22	-0.27	-0.23	0.18	-					
Q_{INIT} [mm]	-0.13	0.00	-0.21	0.52	0.54	0.27	-0.28	0.26	-				
Q_{FAST} [mm]	**0.77**	0.58	**0.80**	-0.17	-0.16	-0.08	0.43	0.33	-0.01	-			
$P_{DURATION}$ [min]	0.56	0.38	**0.62**	-0.59	-0.52	-0.48	0.44	0.14	-0.43	**0.74**	-		
$Q_{DURATION}$ [min]	0.56	0.39	**0.61**	-0.27	-0.27	-0.17	0.42	0.52	0.11	**0.89**	**0.64**	-	
$\Delta_{P/Q}$ [min]	0.13	-0.11	0.29	**-0.71**	**-0.71**	-0.58	0.59	0.41	-0.33	0.52	**0.81**	**0.60**	-
RC [-]	0.31	0.13	0.40	-0.25	-0.29	-0.22	0.44	**0.65**	-0.05	**0.81**	**0.67**	**0.80**	**0.72**

https://doi.org/10.5194/hess-2020-371
Preprint. Discussion started: 3 August 2020

Hydrology and Earth System Sciences
Discussions

Table 4. Correlations between distance metrics for the 14 events with streamflow reaction (after discarding the 24 July event). Absolute values equal or over 0.60 are in bold. For correlations covering all rainfall events, see the part 1 of the supplementary material.

		D_{HILLS}	D_{HILLS}	D_{STREAM}	D_{STREAM}	D_{HAND}	D_{HAND}	D_{HILLS}	D_{STREAM}	D_{HAND}
	River network	*Wet*	*Dry*	*Wet*	*Dry*	*Wet*	*Dry*	*Composite*	*Composite*	*Composite*
D_{HILLS}	*Wet*	-								
D_{HILLS}	*Dry*	**0.96**	-							
D_{STREAM}	*Wet*	0.59	**0.61**	-						
D_{STREAM}	*Dry*	0.54	0.53	**0.99**	-					
D_{HAND}	*Wet*	**0.91**	**0.93**	0.51	0.44	-				
D_{HAND}	*Dry*	**0.75**	**0.89**	0.40	0.28	**0.90**	-			
D_{HILLS}	*Composite*	0.42	0.45	0.08	0.04	0.51	0.49	-		
D_{STREAM}	*Composite*	0.32	0.31	**0.75**	**0.77**	0.18	0.09	-0.57	-	
D_{HAND}	*Composite*	0.26	0.30	-0.05	-0.10	0.40	0.42	**0.98**	**-0.68**	-
RC		-0.20	-0.21	0.10	0.13	-0.28	-0.28	**-0.70**	0.53	**-0.70**
$\Delta_{P/Q}$		-0.10	-0.05	0.21	0.21	-0.13	-0.06	**-0.66**	**0.60**	**-0.68**

https://doi.org/10.5194/hess-2020-371
Preprint. Discussion started: 3 August 2020

Hydrology and Earth System Sciences
Discussions

Table 5. List of the tested predictors for the RC with a pure quadratic regression, and their corresponding statistics: root mean square error (RMSE), coefficient of determination (R^2), variance of residuals (var. residuals), p-value, corrected Akaike criterion (AICc) and AICc ranking. The acceptable p-values (≤0.05) and first 3 ranks are highlighted. The analysis is over 14 events (without the outlier event of 24-Jul).

Predictor 1	Predictor 2	RMSE	R^2	var. residuals	p-value	AICc	rank AICc
P_{ALL}	-	0.34	0.14	0.10	0.44	-24.96	17
P_{NORTH}	-	0.36	0.02	0.11	0.88	-23.20	18
P_{SOUTH}	-	0.31	0.28	0.08	0.17	-27.44	12
I_{ASYM}	-	0.33	0.22	0.09	0.25	-26.37	16
$W_{3\ days}$	-	0.27	0.48	0.06	**0.03**	-31.90	7
D_{HILLS} (composite)	-	0.26	0.52	0.06	**0.02**	-33.00	**3**
D_{STREAM} (composite)	-	0.23	0.61	0.04	**0.01**	-36.13	**1**
P_{ALL}	I_{ASYM}	0.33	0.35	0.07	0.36	-19.88	19
P_{NORTH}	I_{ASYM}	0.34	0.29	0.08	0.50	-18.53	21
P_{SOUTH}	I_{ASYM}	0.33	0.35	0.07	0.37	-19.84	20
$W_{3\ days}$	I_{ASYM}	0.25	0.62	0.04	**0.05**	-27.38	13
D_{HILLS} (composite)	I_{ASYM}	0.23	0.68	0.04	**0.03**	-29.55	9
D_{STREAM} (composite)	I_{ASYM}	0.25	0.62	0.04	**0.05**	-27.30	14
P_{ALL}	D_{HILLS} (composite)	0.22	0.70	0.03	**0.02**	-30.65	8
P_{NORTH}	D_{HILLS} (composite)	0.26	0.60	0.05	0.06	-26.76	15
P_{SOUTH}	D_{HILLS} (composite)	0.21	0.74	0.03	**0.01**	-32.80	4
$W_{3\ days}$	D_{HILLS} (composite)	0.24	0.65	0.04	**0.04**	-28.34	11
P_{ALL}	D_{STREAM} (composite)	0.20	0.75	0.03	**0.01**	-33.18	**2**
P_{NORTH}	D_{STREAM} (composite)	0.21	0.74	0.03	**0.01**	-32.55	5
P_{SOUTH}	D_{STREAM} (composite)	0.21	0.74	0.03	**0.01**	-32.46	6
$W_{3\ days}$	D_{STREAM} (composite)	0.24	0.67	0.04	**0.03**	-29.10	10

https://doi.org/10.5194/hess-2020-371
Preprint. Discussion started: 3 August 2020

Hydrology and Earth System Sciences
Discussions

Table 6. List of the tested predictors for the lag $\Delta_{P/Q}$ with a pure quadratic regression, and their corresponding statistics: root mean square error (RMSE), coefficient of determination (R^2), variance of residuals (var. residuals), p-value, corrected Akaike criterion (AICc) and AICc ranking. The acceptable p-values (≤0.05) and first 3 ranks are highlighted. The analysis is over 14 events (without the outlier event of 24-Jul).

Predictor 1	Predictor 2	RMSE	R^2	var. residuals	p-value	AICc	rank AICc
$P_{max\ ALL}$	-	13.07	0.64	144.52	**0.00**	76.99	**3**
$P_{max\ NORTH}$	-	12.70	0.66	136.56	**0.00**	76.20	**2**
$P_{max\ SOUTH}$	-	16.52	0.43	231.05	**0.05**	83.56	11
I_{ASYM}	-	17.25	0.37	251.75	0.08	84.76	13
$W_{3\ days}$	-	19.83	0.17	332.65	0.35	88.66	19
D_{HILLS} (composite)	-	16.28	0.44	224.27	**0.04**	83.14	10
D_{STREAM} (composite)	-	13.39	0.62	151.71	**0.00**	77.67	4
$P_{max\ ALL}$	I_{ASYM}	11.10	0.79	85.35	**0.00**	78.72	5
$P_{max\ NORTH}$	I_{ASYM}	12.89	0.71	115.01	**0.02**	82.89	8
$P_{max\ SOUTH}$	I_{ASYM}	10.06	0.83	70.06	**0.00**	75.95	**1**
$W_{3\ days}$	I_{ASYM}	15.86	0.57	174.17	0.08	88.70	20
D_{HILLS} (composite)	I_{ASYM}	12.97	0.71	116.52	**0.02**	83.07	9
D_{STREAM} (composite)	I_{ASYM}	13.83	0.67	132.39	**0.03**	84.86	15
$P_{max\ ALL}$	D_{HILLS} (composite)	14.18	0.65	139.25	**0.03**	85.57	17
$P_{max\ NORTH}$	D_{HILLS} (composite)	13.95	0.67	134.65	**0.03**	85.10	16
$P_{max\ SOUTH}$	D_{HILLS} (composite)	16.57	0.53	190.15	0.12	89.93	21
$W_{3\ days}$	D_{HILLS} (composite)	15.65	0.58	169.50	0.07	88.32	18
$P_{max\ ALL}$	D_{STREAM} (composite)	11.40	0.78	89.99	**0.01**	79.46	6
$P_{max\ NORTH}$	D_{STREAM} (composite)	11.55	0.77	92.36	**0.01**	79.82	7
$P_{max\ SOUTH}$	D_{STREAM} (composite)	13.37	0.69	123.70	**0.02**	83.91	12
$W_{3\ days}$	D_{STREAM} (composite)	13.82	0.67	132.18	**0.03**	84.84	14